

Final author response to reviewers of the gmd-2020-189 manuscript

We thank both reviewers for their constructive comments and helpful suggestions to improve our manuscript. Our responses to their comments are provided below, separately for each reviewer (sections A and B). At the end, we provide a third section (C), describing additional changes resulting from our answers to the reviewers' comments, followed by the revised manuscript with changes tracked.

A. Reviewer 1 (Andrew May)

Major comment

Reviewer comment:

“There appears to be a fundamental error regarding the volatility (C_i^*) of levoglucosan in this modeling framework. Table S1 shows that $C_i^* = 3 \times 10^{-3} \text{ kg m}^{-3} = 3 \times 10^6 \text{ } \mu\text{g m}^{-3}$, which would imply that that vast majority of the levoglucosan should be in the gas phase (e.g., if COA = $30 \text{ } \mu\text{g m}^{-3}$, 99.999% would be in the gas phase). This does not match with the initial distribution of the gas-phase and aerosol-phase concentration in Table S1. Experimentally, we showed that this was more like $13 \text{ } \mu\text{g m}^{-3}$ in May et al. (2012). We speculated that this was why Hennigan et al. (2010) observed uptake coefficients (γ) greater than 1, and this could be a plausible explanation for the results in Knopf et al. (2011) for NO_3 radicals. Moreover, a structure-activity relationship (Mansouri et al., 2018) predicts a vapor pressure that yields $C_i^* \approx 1 \text{ } \mu\text{g m}^{-3}$. Perhaps this issue with C_i^* is the reason why $\alpha = 0.0001$ is required to demonstrate good agreement in Figure 1?”

Author comment:

Indeed, the C_i^* value we used in our model is likely too large and we thank the reviewer for pointing this out. In our model we used the maximum value of a range from May et al. (2013). However, levoglucosan may have a C_i^* value closer to the lower end of that range, since it is not very volatile.

To address this, we ran new simulations by considering both suggestions ($C_i^* = 13 \text{ } \mu\text{g m}^{-3}$ and $C_i^* = 1 \text{ } \mu\text{g m}^{-3}$). We confirm that the model also predicts well the LEV degradation at larger α values than 0.001, respectively 0.01 and 0.1 (using $C_i^* = 13 \text{ } \mu\text{g m}^{-3}$) and 1.0 (using $C_i^* = 1 \text{ } \mu\text{g m}^{-3}$). The variations in the α response to C_i^* are driven by the different experimental conditions used to initialize the model. For example, using conditions from Hennigan et al. (2010), the model performed well at $\alpha = 0.1$ ($C_i^* = 13 \text{ } \mu\text{g m}^{-3}$) and at $\alpha = 1.0$ ($C_i^* = 1 \text{ } \mu\text{g m}^{-3}$). Conditions from Lai et al. (2014) worked well only at $\alpha = 0.01$ ($C_i^* = 13 \text{ } \mu\text{g m}^{-3}$). However, we chose to report results only for cases when $C_i^* = 13 \text{ } \mu\text{g m}^{-3}$ was used because this value worked well with respect to α , model evaluation and model performance, for all the modeled scenarios, including the conditions from an additional experimental study that the reviewer has suggested (Pratap et al., 2019). These results are shown in revised Figures 1 and 2 below. Model performance was not negatively affected; on the contrary, the accuracy improved slightly (from 48% to 47%).

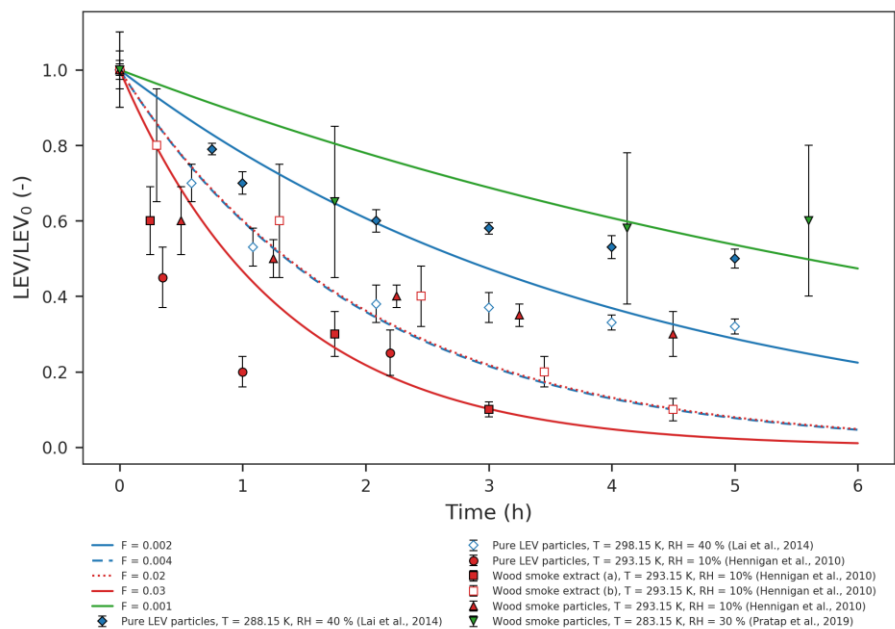


Figure 1 Simulated LEV degradation (lines) and measured LEV degradation (points); Color represents conditions from different chamber experiments taken from three studies (red – Hennigan et al. (2010), blue – Lai et al. (2014) and green – Pratap et al. (2019)) used in the simulations. LEV concentration is normalized by the initial concentration (LEV/LEV_0).

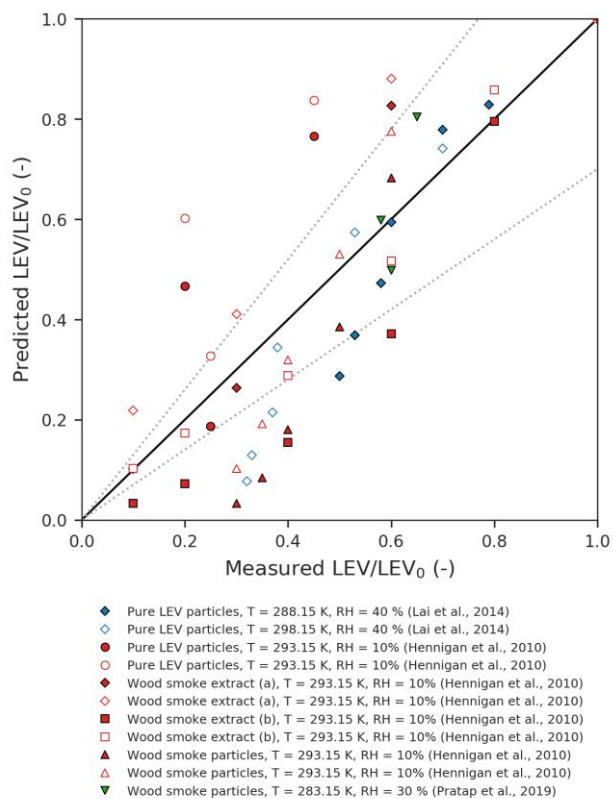


Figure 2 Parity plot of predicted versus measured LEV concentration (normalized by the initial concentration). The dotted lines represent the $\pm 30\%$ error margins.

General comment

Reviewer comment:

“Related to the Major Comment, Kulmala and Wagner (2001) provide a theoretical relationship between mass accommodation coefficients (α) and γ . One key point that they make is that $\alpha \geq \gamma$ (depending on the Knudsen number). In this work, $\gamma \gg \alpha$, based on Table 2. Therefore, the authors should either constrain $\alpha > 0.1$ or provide some justification for $\alpha \ll \gamma$. I suspect that this issue may work itself out once the Major Comment has been resolved, but it is worth noting in the event that it does not.”

Author comment:

We confirm that by correcting the C_i^* used in our model, we obtained good model predictions at α values that are 1-2 orders of magnitude larger compared to previous simulations at much larger C_i^* values (see our response to the major comment above). These α values (0.01 and 0.1) are still smaller than those of the uptake coefficients (γ) for most of the chemical species, including for levoglucosan. However, as seen in Table 2, the great majority of the γ values were computed in this study, in the absence of their experimental measurements. In eq. 7, we assume a similar 2nd order heterogeneous reaction rate for all the species (see line 165); this may bias our calculations of γ towards larger values. For γ values on the order of 10^{-1} (OH uptake by levoglucosan, for example) and Knudsen numbers on the order of 10^{-1} (all modeled cases), the corresponding α should be 0.1, according to Fig. 1 in Kulmala and Wagner (2001). This is true when we model conditions from Hennigan et al. (2010); thus, in this case the $\alpha \geq \gamma$ criterion is satisfied. Modeled conditions from Lai et al. (2014) and Pratap et al. (2019) do not meet this criterion for levoglucosan because, for similar Kn and γ values, the model worked well (compared to experimental data) only at $\alpha = 0.01$; in these cases, $\alpha < \gamma$. However, for other species with smaller γ (O_3 and N_2O_5), all the modeled cases in our study satisfy the criterion $\alpha \geq \gamma$. It is worth noting here that the effective α values we found in our study, by comparing model predictions with data, have inherent uncertainties associated with both the data and the model.

To address this reviewer’s comment directly in the manuscript:

(i) We introduce the relationship between α and γ described by Kulmala and Wagner (2001) by rephrasing the sentence on line 205:

“The mass accommodation coefficient is related to the G/P partitioning mechanism (eq. 14) and the uptake coefficient (γ). Theoretically, $\alpha \geq \gamma$, depending on the Knudsen number (Kulmala and Wagner, 2001).”

ii) We discuss our results with respect to α and γ by adding the following paragraph starting on line 226:

“These α values are smaller than those of γ for most of the chemical species, including for levoglucosan. However, as seen in Table 2, the great majority of the γ values were computed in this study, in the absence of their experimental measurements. In eq. 7, we assume a similar 2nd order heterogeneous reaction rate for all the species; this may bias our calculations of γ towards larger values. For γ values on the order of 10^{-1} (OH uptake by levoglucosan, for example) and Knudsen numbers on the order of 10^{-1} (all modeled cases), the corresponding α should be ~ 0.1 , according to Fig. 1 in Kulmala and Wagner (2001). This is true when we model conditions from Hennigan et al. (2010); thus, in this case the $\alpha \geq \gamma$ criterion is marginally satisfied. Modeled conditions from Lai et al. (2014) and Pratap et al. (2019) do not meet this criterion for levoglucosan because, for similar Kn and γ values, the model worked well (compared to experimental data) only at $\alpha = 0.01$; in these cases, $\alpha < \gamma$. However, for other species with smaller γ (O_3 and N_2O_5), all the modeled cases in our study satisfy the criterion $\alpha \geq \gamma$. It is worth noting here that the effective α values we found in our study by comparing model predictions with data have inherent uncertainties associated with both the data and the model.”

Specific comments

Reviewer comment:

“Lines 198-203: As I’m reflecting on this after having read the full draft, it seems like these “F” values could be related to the mass fraction of levoglucosan in the particles. For example, $F = 0.03$ is the slope of “ m/z 60” (proxy for anhydrosugars in the Aerosol Mass Spectrometer world) vs. OA concentration in Figure 7 in Sullivan et al. (2014). I haven’t carefully read through Lai et al. (2014), but conceivably, they could have used lower mass-mixing ratios of levoglucosan in their particles. I bring this up because as written, F essentially sounds like a “fudge factor” to get the model to agree with observations. Maybe something like “We expect F to be, at a maximum, 0.1 due to observed mass fractions in biomass burning organic aerosol”

Author comment:

This is an interesting suggestion. We used F precisely for accounting for the fact that there are many factors that may inhibit heterogeneous chemistry while the heterogeneous reaction rate ($k_{SFC_REACTION}$) does not account for that. Model evaluation confirms that by not constraining $k_{SFC_REACTION}$ by F, results are not realistic. We see that F could be a mass fraction accounting for levoglucosan (or other particle-phase species) that is available to react with gas-phase oxidants. At a minimum, we found F to be 0.001 (conditions from Pratap et al., 2019), while at a maximum, F was 0.02-0.03 (conditions from Hennigan et al., 2010) (see Figure 1 above). We also think that these variations in F are driven by different temperature (and possibly relative humidity) conditions modeled, with higher temperature sustaining larger F and lower temperature supporting lower F. Therefore, we added your suggestion starting on line 202 and we adjusted the next sentence to accommodate this addition as follows:

“We expect F to be, at a maximum, 0.1 due to observed mass fractions in biomass burning organic aerosols (Sullivan et al., 2014). However, for sensitivity analysis, we varied F from 1.0 (default case) to lower values (0.1, 0.01 and 0.001) to slow down the heterogeneous reaction rates.”

Reviewer comment:

“Lines 203-204: I have no recollection of making this claim regarding α in May et al. (2013), and quickly reviewing that paper, it appears that the closest thing to that is that there appeared to be no mass transfer limitations for the evaporation of biomass burning smoke. In May et al. (2012), we did include some discussion of this in the online supporting information, but that was more focused on the fact that even if we decrease $\alpha < 1$, the evaporation timescale is shorter than heterogeneous chemistry timescale. I guess that my point here is that my previous work has been mis-interpreted.

These results, coupled with $\gamma \approx 1$ (presumably, based on Kessler et al. (2010)?) and Kulmala and Wagner (2001) suggesting that $\alpha \geq \gamma$, seem to imply that $\alpha \approx 1$.”

Author comment:

On Line 204, we refer to α as “...(which is 0.1 for a system in equilibrium (May et al., 2013)...”. We inferred this from paragraph 18/page 11,330 (May et al., 2013), where $\alpha \geq 0.1$ is considered a good value for a system in equilibrium, as has been found in different chamber systems. We rephrased the sentence starting on line 203 as follows:

“In addition, we varied the mass accommodation coefficient (see eq. 14) from a default case of 0.1 (which is the lower limit of α for a system in equilibrium (May et al., 2013)) to lower values (0.01 and 0.001) and larger values (1.0). It was necessary to vary α because its value is unknown for levoglucosan and its degradation products.”

Reviewer comment:

“Section 3.2 and Figure 4: I am a bit confused by this discussion about yield, which is perhaps based on an *a priori* expectation that SOA yield increases with increased photochemical aging. Is the implication that initially, many of the oxidation products remain in the particle phase ($t < \sim 6$ hr) but as the chemistry continues, heterogeneous oxidation results in more volatile products until a steady-state is reached (at $t \sim 24$ -36 hrs?)”

Author comment:

If we look at Figures S3-S7 (see section C/Supplemental Information), about the same number of products (~ 3) is present in both phases, but the products differ between the two phases. Heterogeneous chemistry is the driver of these yields in the first hours. Condensation is negligible, since LEVP4, which is a product of gas-phase chemistry only, is not present in the aerosol phase; it only appears in the aerosol phase at the end of the simulation, in some cases (Fig. S4-S7). Evaporation is not important either since the products LEVP6 and LEVP7, generated by heterogeneous chemistry only, are not seen in the gas phase at all. Most of the oxidation products in the aerosol phase remain in the aerosol phase over the entire simulation period, except for LEVP5 and LEVP1 that may partition to the gas phase after 6 hours. The steady-state is reached because the concentration of precursors is near-zero and the oxidation products from heterogeneous chemistry and condensation (i.e., LEVP4 only) remain in the aerosol phase. So, yes, your interpretation is correct. Therefore, we supplemented this section by adding the following text starting on line 274 (for updated Figure 4, see section C/Manuscript):

“These high SOA yields in the first 6 hours are the result of rapid conversion of the precursors to aerosol-phase products, mainly due to heterogeneous chemistry. Because these products are not seen in the gas phase, evaporation does not influence the SOA yields in this early stage of the simulation; condensation of gas-phase products (LEVP4 and LEVP5) is also negligible (see Fig. S3-S7). Most of the oxidation products remain in the aerosol phase over the entire simulation period, except for LEVP5 and LEVP1 that may partition to the gas phase. SOA yield reaches steady-state at ~ 24 -26 hours due to near-zero concentrations of the two precursors and the presence of oxidation products from heterogeneous chemistry and G/P partitioning (i.e., condensation of LEVP4) in the aerosol phase.”

Suggestion

Reviewer comment:

“Another dataset to consider would be that from Pratap et al. (2019). They also modeled their own data, explicitly accounting for gas-particle partitioning and chamber wall loss in addition to oxidation chemistry, in predicting particle-phase levoglucosan concentrations. If nothing else, these data can provide another valuable test set at colder temperatures than Hennigan et al. (2010) and Lai et al. (2014).”

Author comment:

We thank the reviewer for this suggestion. We considered it in our simulations (see revised Figs. 1 and 2 above). Because conditions of this study represent wintertime conditions ($T = 10^{\circ}\text{C}/283.15$ K), the model line falls in the proximity of the model conditions from Lai et al. (2014) ($T = 15^{\circ}\text{C}/288.15$ K) and works for an F of similar magnitude (10^{-3}) and α (0.01). We also refer to this study in the manuscript and Supplemental Information (see section C for additional changes). Simulation results based on this study are also included in Figs. 3 and 4 (see section C/Manuscript) and Fig. S7 (see section C/Supplemental Information).

B. Reviewer 2 (anonymous)

Suggestion

Reviewer comment:

“I would highly encourage the authors to try out their model on ambient levoglucosan data from aircraft campaigns that were able to follow smoke plumes over time such as WINTER and WECAN.”

Author comment: This is a great suggestion and thank you for pointing out the two field studies. We thought about testing the model in 1-D or 2-D modeling settings prior to implementing the LEVCHEM_v1 mechanism into a 3-D modeling framework, but this required an additional model development focus and setup that was beyond the goal of this study. However, we will still consider applying LEVCHEM_v1 to fire plumes in the future.

General Comments

Reviewer comment:

“In the paper it seems to go back and forth if it is written as gas-phase and aerosol-phase (with hyphens) or gas phase and aerosol phase (without hyphens). This should be checked throughout the entire text.”

Author comment:

There are situations when the hyphen is needed and situations when the hyphen is not needed; this is not necessarily incorrect even if it appears to be inconsistent throughout the text. When we use it as an adjective (i.e. gas-phase reaction), we think that the hyphen is needed. When we use it differently (i.e., “it happens in the gas phase”), we do not think the hyphen is needed. Therefore, we made no changes in the text regarding this apparent issue, except for the title of Table 1 (see the manuscript at the end of this author response).

Specific Comments

Reviewer comment

Line 73 – Suggest adding an of after developed use

Author comment

Thank you for pointing this out. In addition, the word “use” was not supposed to be there. Therefore, we corrected this part to read as “Here we developed a zero-dimensional (0-D) modeling framework...”.

Reviewer comment

Line 173 – Suggest changing particle phase to particle-phase

Author comment

We did not follow this suggestion (see our motivation above).

Reviewer comment

Line 260 – The comma after Supplemental Information) should be a period

Author comment

We corrected this.

Reviewer comment

Line 340 – There is an extra space in gas-phase

Author comment

We corrected this.

Reviewer comment

Line 393 – In the Alvarado et al. reference, periods are missing in the initials for author Akagi

Author comment

We corrected this.

Reviewer comment

Line 394 – In the Arangio et al. reference, believe oh should be capitalized

Author comment

We corrected this.

Reviewer comment

Figure 3 -In the plot titles, the hyphen is missing in Gas-phase and Aerosol-phase

Figure 8 -In the plot titles, the hyphen is missing in Gas-phase and Aerosol-phase

Figures S3, S4, S5, S6 -In caption, the hyphen is missing in gas-phase and aerosolphase

Author comment

We accepted your suggestion for Figures 3 and 8 titles, because the use of the hyphen was justified in these cases (see section C). However, we do not think that a hyphen is needed in the captions of Figures S3 to S6 (and the new Fig. S7), for the reason we have already discussed (see our comment above).

C. Other revisions

In this section, we explicitly provide additional changes in the Manuscript and Supplemental Information resulting from our answers to reviewers' comments (see sections A and B).

Manuscript

Revisions of the manuscript include:

Line revisions (lines correspond to those in the original manuscript)

Line 10: We removed the extra space between “of” and “a”.

Line 16: We added “gas-phase” between “with” and “degradation”.

Line 17: We replaced “3.5 days” by “5 days” and “8-21 hours” by “8-36 hours”.

Lines 18-20: We rephrased this sentence to point out the conditions tested in the sensitivity analysis and to adjust the text in response to the change made on line 17:

“We varied the heterogeneous reaction rate constant in a sensitivity analysis (for summer conditions only) and found that longer degradation time scales of LEV are possible, particularly in the aerosol phase (7 days), implying that some LEV may be transported regionally.”

Line 25: Based on new simulations, we updated the range of SOA yields “5 to 32%” by “4 to 32%”.

Line 28: We deleted “(VOC)”.

Line 30: Because we modeled experimental conditions from an additional study (Pratap et al., 2019), which extend to 5.6 hours, we replaced “3-5 hours” by “3-6 hours”.

Line 56: We added “; Pratap et al., 2019” to the references cited on this line.

Line 57: We replaced “character” by “chemistry”.

Line 60: To acknowledge the previous works of Pratap et al. (2018, 2019) with respect to modeled gas-particle partitioning and multiphase chemistry of levoglucosan, we added the following sentence starting on this line:

“Previous studies applied the gas-particle partitioning model of May et al. (2013) to levoglucosan but its multiphase chemical decay was limited to the reaction with the OH radical only (Pratap et al., 2018; 2019).”

Lines 61 and 325-326: We corrected “modelled” by “modeled”.

Line 68: We added a hyphen to the word gas.

Line 82: We corrected “form” by “from”.

Line 112: We replaced “outputs” by “information” to avoid using the same word twice in the sentence.

Line 148: We deleted the “or surface area”.

Line 191: We deleted “organic molecules in”.

Lines 207 and 214: We added “; Pratap et al., 2019”

Line 213: We deleted “one”.

Line 224: We replaced “5 hours” by “5-6 hours” because data from Pratap et al. (2019) extends to 5.6 hours.

Lines 224-226: We rephrased the sentence on these lines to include changes in F and α based on new simulations in response to reviewer 1’s major comment:

“Overall, the model predicted that LEV degradation closely follows the measured LEV degradation in relatively slower heterogeneous chemistry scenarios ($F = 0.001; 0.002; 0.004; 0.02; 0.03$, depending on the experimental data considered) and at mass accommodation coefficients of 0.1 and 0.01.”

Line 229: We added “Pratap et al. (2019)”.

Line 235: We corrected “versus” from italic to non-italic.

Lines 236-237: We corrected the sentence to include the modeled scenario in green “scenarios (red, blue and green)”.

Lines 238-239: Based on new simulations, we corrected “48%” by “47%”.

Line 241: We replaced “five” by “5-6”, since data from Pratap et al. (2019) extends slightly beyond 5 hours.

Lines 242-243: Based on new simulations, we replaced “1.5-3.5 days” by “1.5-5 days” and “8-21 hours” by “8-36 hours”. We also added on line 242 the word “nearly” since the concentration of LEV was not zero after this time scales.

Lines 246-247: We replaced “5 hours” by “5-6 hours”.

Line 247: We replaced “Figure S4” by “Figure S7”.

Line 254: We replaced “5 hours” by “5-6 hours”.

Lines 259-264: We deleted the text on these lines as we found it not so relevant.

Line 365: We replaced “nitrogen cycle” by “nitrogen cycling” and “carbon cycle” by “carbon cycling”.

Line 273: We replaced “1-12 minutes” by “2-34 minutes”.

Line 274: Based on new simulations, we updated the range of SOA yields “5 to 32%” by “4 to 32%”.

Lines 274-277: Based on new simulations, we revised the text on these lines as follows:

“Among the simulated scenarios, the largest SOA yields resulted when higher initial LEV_A concentrations were used in the simulations and they did not decrease below 8% in wintertime conditions (Figure 4a and Table S1). The heterogeneous chemistry was the slowest for SOA yields predicted for winter conditions (suggested by $F = 0.001$) while it was the fastest for those associated with summer conditions ($F = 0.02-0.03$).”

Lines 277-278: Based on new simulations, we corrected the total aerosol mass described on these lines as follows:

“The total aerosol mass (the sum of concentrations of all LEV-related aerosol species, including the radicals) also increased by 8-15% in the first six hours and kept increasing, although at a slower pace, to up to 18-29% at the end of the simulation period. The smallest total aerosol mass in the first six hours (8%) was observed in modeled wintertime conditions, while the highest total aerosol mass (14-15%) was observed in summertime conditions.”

Line 278: We adjusted the beginning of the sentence starting on this line as “These suggest that...”.

Lines 302-303: Based on new simulations, we corrected the linear slopes of O₃ vs. NO_x and O₃ vs. VOC as follows:

“...(linear slope of -0.250 ± 0.001 ppb/ppbC) but not as much as NO_x did (linear slope of -2.821 ± 0.007 ppb/ppb)...”.

Line 304: Based on new simulations, we corrected the concentration of O₃ mentioned on this line from “117 ppb” to “112 ppb”.

Line 315: We corrected the α value from 0.001 to 0.1 to reflect the conditions which were re-modeled in response to reviewer 1’s major comment.

Lines 316-318: Based on new simulations, the comparison made on these lines does hold only for aerosol-phase levoglucosan. Therefore, we reformulated the sentence as:

“While the time scale of gas-phase LEV is similar (5 days) to that observed with reaction rates used in chamber comparisons (see section 3.1), the time scale of aerosol-phase LEV is much larger (7 days versus 36 hours), suggesting that LEV associated with PM can be transported and deposited regionally.”

Line 313: We rephrased the sentence starting on this line to reflect the new results:

“Over these time scales, SOA yields vary roughly within the same range (14-33%) as observed in the previous cases considered (see section 3.2).”

Lines 322-326: Based on new simulations, we also adjusted the text on these lines as follows:

“We also tested the sensitivity of the mass accommodation coefficient (α) at $F = 0.01$, using conditions from Hennigan et al. (2010). Varying α by four orders of magnitude (0.001, 0.01, 0.1 and 1.0) showed little effect on LEV degradation (i.e., degradation in the gas phase was slightly faster when $\alpha = 1$, while degradation in the aerosol phase was slightly faster when $\alpha = 0.001-0.1$) in comparison to the effect of slowing down the heterogeneous chemistry (F , as described above). The effect of the mass accommodation coefficient on LEV degradation appears to be more important when the G/P partitioning is modeled as gas-aerosol equilibrium reactions of which the partitioning coefficient is modeled with eq. 13.”

Lines 337-343: Based on new simulations, we adjusted the text on these lines as follows:

“We found that LEV degradation time scale ranges from 8-36 hours (aerosol-phase) to 1.5-5 days (gas-phase); however, model output was evaluated only for six hours through comparison to chamber measurements. In addition, we conducted a sensitivity analysis investigating a factor slowing down the heterogeneous chemistry and found that longer degradation time scales may occur, particularly in the aerosol phase (7 days). This longer time scale is slightly larger

than that of deposition (1-5 days) but is slightly shorter than that of regional transport (10 days), suggesting that some fraction of aerosol-phase LEV may be transported regionally.”

Lines 347-352: Based on new simulations, we updated the text on these lines to reflect the new findings as follows:

“LEV degradation contributes to SOA formation that was quantified mainly through simulated SOA yields. Based on 6-h degradation time scales, simulated SOA yields ranged from 4 to 32% and peaked in the first 2-34 minutes. Varying the heterogeneous chemistry rate by four orders of magnitude did not result in significantly different SOA yields (14-33%). The total PM mass (determined as the ratio of total aerosol concentration to initial LEV_A concentration) increased by 8-15% in the first six hours of all simulations and continued to slowly increase to 18-29% at the end of the simulation period.”

Line 359: We replaced “117 ppb” by “112 ppb”.

Line 383: We replaced the link to the source of LEVCHEM_v1 model files “<https://zenodo.org/record/3885786>” by “<https://zenodo.org/record/4215973>”. This new link stores the model files representing simulation setups, inputs and outputs of the new simulation runs in response to reviewer’s 1 major comment.

Reference revisions

We added four new references to this section:

Kulmala, M. and Wagner, P. E.: Mass accommodation and uptake coefficients - a quantitative comparison, *J. Aerosol Sci.*, 32, 7, 833–841, [https://doi.org/10.1016/S0021-8502\(00\)00116-6](https://doi.org/10.1016/S0021-8502(00)00116-6), 2001.

May, A. A., Saleh, R., Hennigan, C. J., Donahue, N. M. and Robinson, A. L.: Volatility of organic molecular markers used for source apportionment analysis: measurements and implications for atmospheric lifetime, *Environ. Sci. Technol.*, 46, 22, 12435-12444, <https://doi.org/10.1021/es302276t>, 2012.

Pratap, V., Chen Y., Yao G. and Nakao S.: Temperature effects on multiphase reactions of organic molecular markers: A modeling study, *Atmos. Environ.*, 179, 40-48, <https://doi.org/10.1016/j.atmosenv.2018.02.009>, 2018.

Pratap, V., Bian, Q., Kiran, S. A., Hopke, P. K., Pierce, J. R. and Nakao, S.: Investigation of levoglucosan decay in wood smoke smog-chamber experiments: The importance of aerosol loading, temperature, and vapor wall losses in interpreting results, *Atmos. Environ.*, 199, 224–232, <https://doi.org/10.1016/j.atmosenv.2018.11.020>, 2019.

We corrected most of the references by: (1) adding “and” before the last author, (2) adding space between author initials and (3) adding the period to the abbreviated journal names.

Figure revisions

Figure 3: We updated this figure (and its caption) based on our response to “Major comment” and “Suggestion” of reviewer 1 and suggestion from reviewer 2. It shows that degradation timescale of levoglucosan increases in both phases (gas-phase: from 1.5-3.5 days to 1.5-5 days; aerosol-phase: from 8-21 hours to 8-36 hours) but only because of the inclusion of Pratap et al. (2019) “wintertime” conditions in the simulations (purple dotted line). The effect of using much smaller C_i^* values in the simulations is reflected by the larger α values (0.01-01 compared to 0.001) which were found to be effective, according to the data.

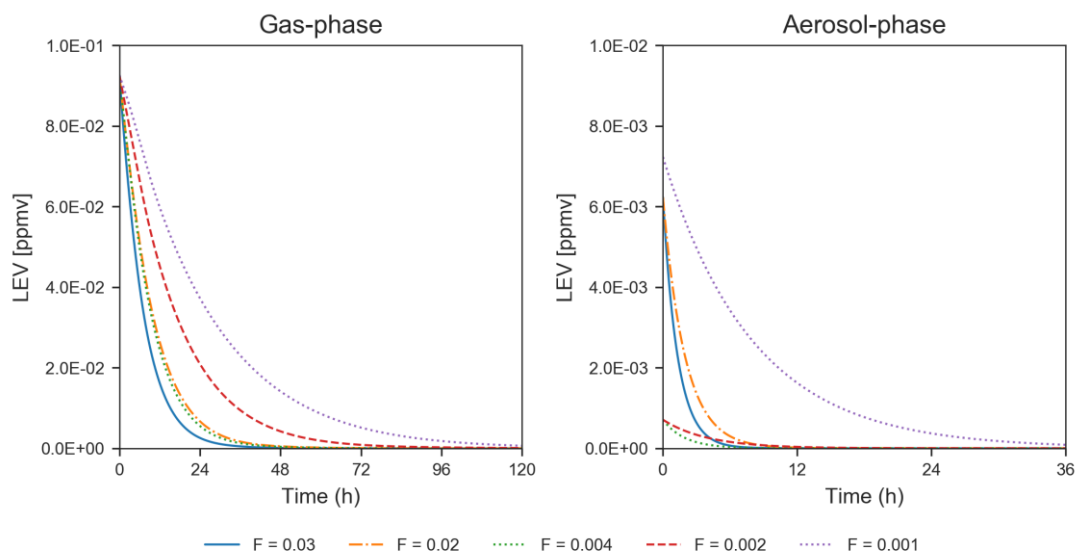


Figure 3 Degradation of LEV (conditions from Hennigan et al. (2010) when $F=0.02-0.03$ and $\alpha = 0.1$, from Lai et al. (2014) when $F=0.002-0.004$ and $\alpha = 0.01$, and from Pratap et al. (2019) when $F = 0.001$ and $\alpha = 0.01$). Note the change in the scale of the axes between the two panels.

Figure 4: We updated this figure (and its caption) based on our response to the “Major comment” and “Suggestion” of reviewer 1. No significant changes compared to original Figure 4 are observed, except for the fact that Figure 4a additionally includes the modeled conditions from Pratap et al. (2019) (see the dotted purple line).

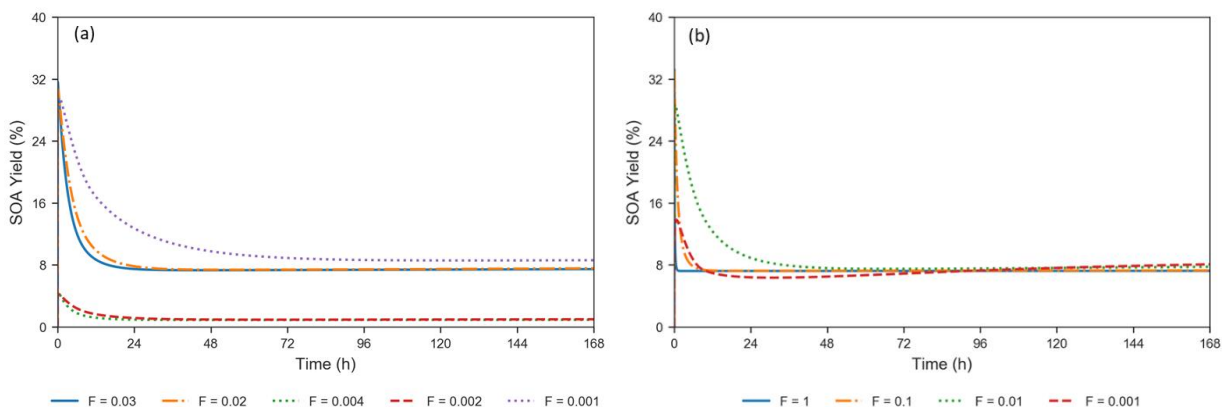


Figure 4 (a) Evolution of SOA yields from LEV degradation using valid simulations (conditions from Hennigan et al. (2010) when $F=0.02-0.03$ and $\alpha = 0.1$, from Lai et al. (2014) when $F=0.002-0.004$ and $\alpha = 0.01$), and from Pratap et al. (2019) when $F = 0.001$ and $\alpha = 0.01$). (b) Effect of varying the heterogeneous reaction rate coefficient by 4 orders of magnitude, at constant mass accommodation coefficient ($\alpha = 0.1$) (conditions from Hennigan et al. (2010)).

Figures 5-7: The plotted information in these figures did not change significantly. However, because we re-ran simulations in response to reviewer’s 1 comment (see section A) and included conditions from an additional data set (Pratap et al., 2019), we re-plotted the results in these figures (see below) and replaced the figures in the original manuscript.

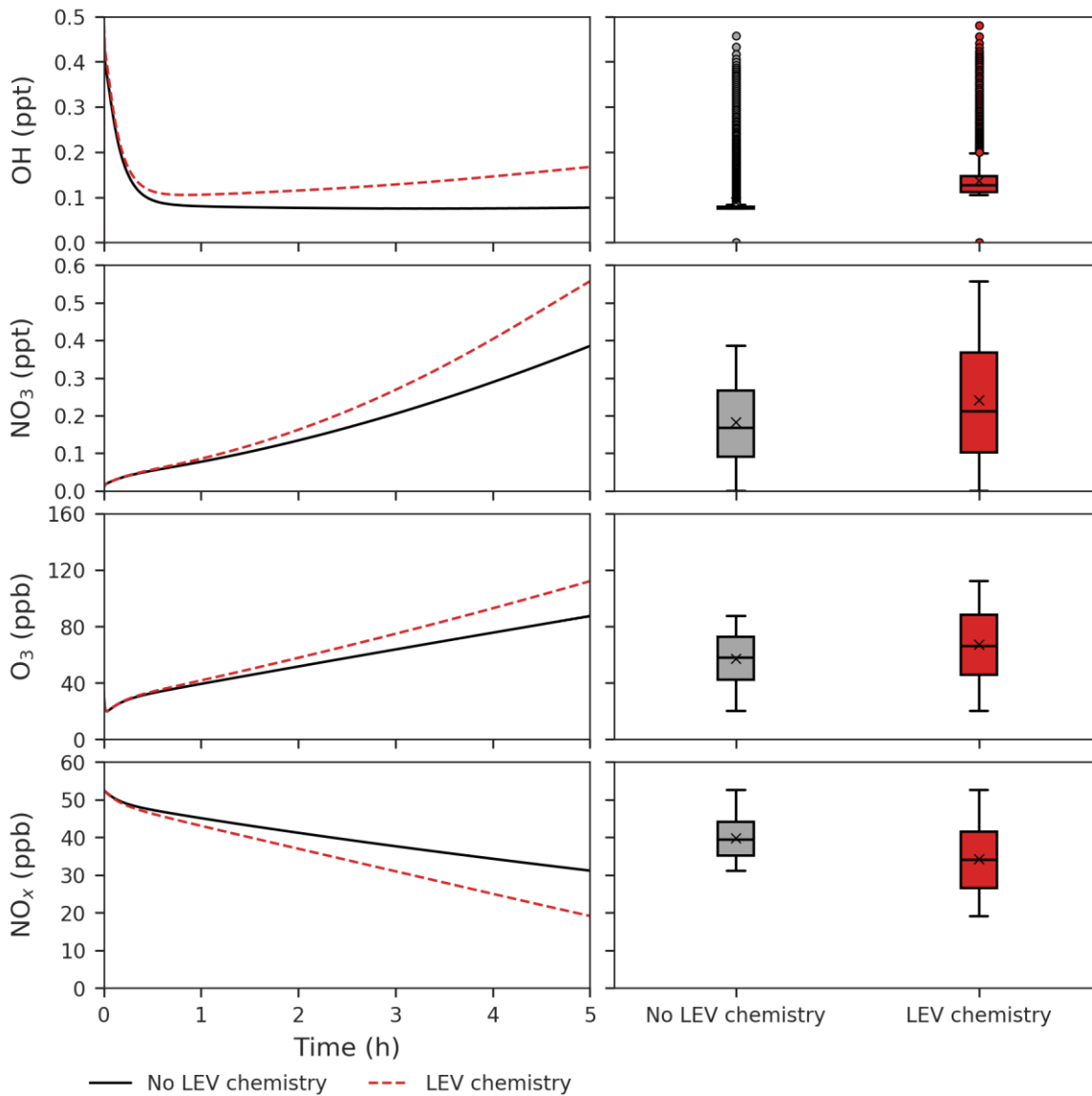


Figure 5 Effects of LEV chemistry on OH, NO₃, O₃ and NO_x (in red, relative to the case without LEV chemistry shown in black or grey). The time series represent averages of simulations performed with LEV chemistry (dashed red line) and without LEV chemistry (black line) over the 5-h time scale. The box plots show the distributions of the species concentration for the entire 5 hours. Note that findings shown here are determined over a range of F values depending on experimental conditions.

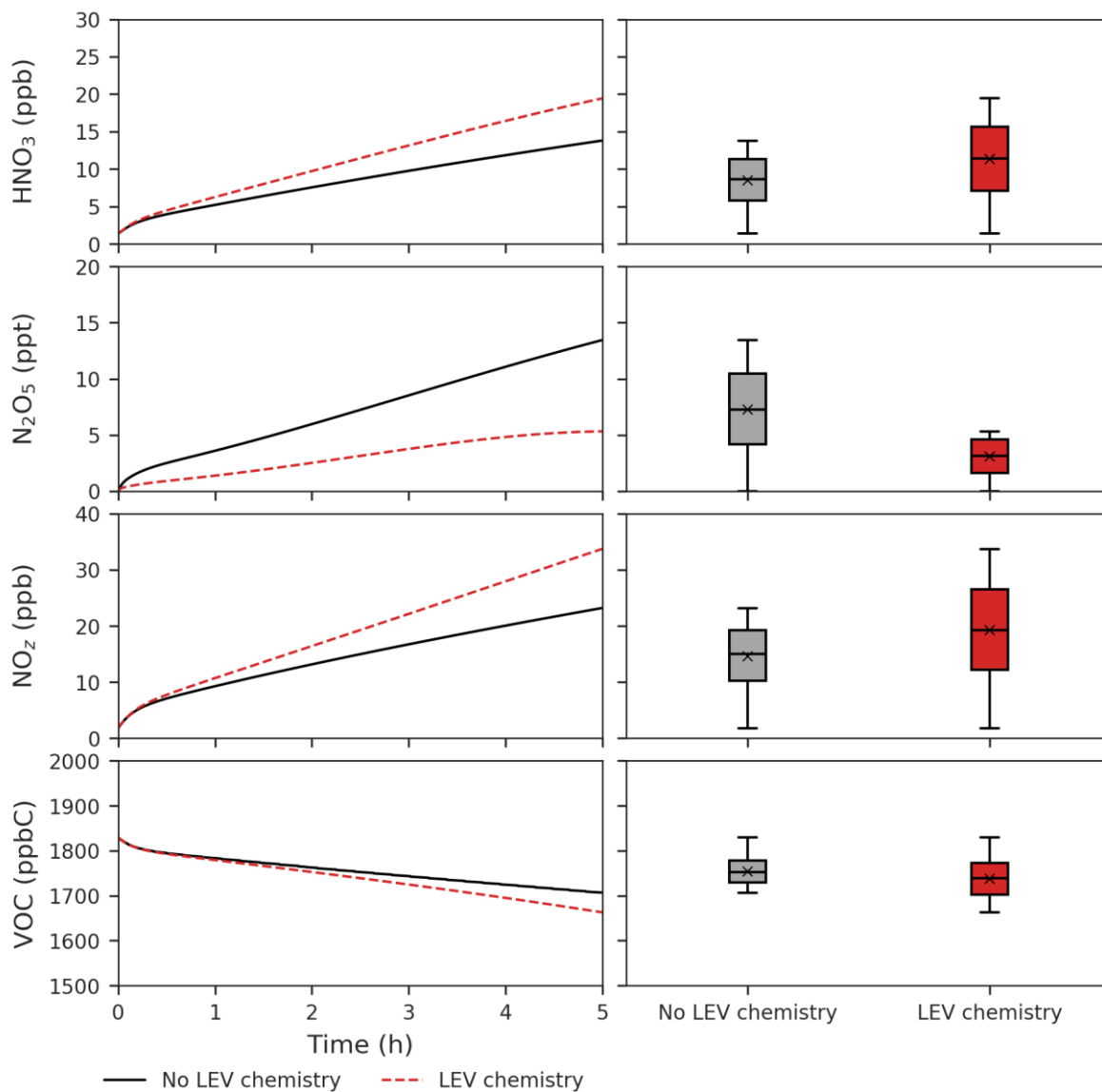


Figure 6 Effects of LEV chemistry on HNO₃, N₂O₅, NO_z and VOC (in red, relative to the case without LEV chemistry shown in black or grey). The time series represent averages of simulations performed with LEV chemistry (dashed red line) and without LEV chemistry (black line) over the 5-h time scale. The box plots show the distributions of the species concentration for the entire 5 hours. Note that findings shown here are determined over a range of F values depending on experimental conditions.

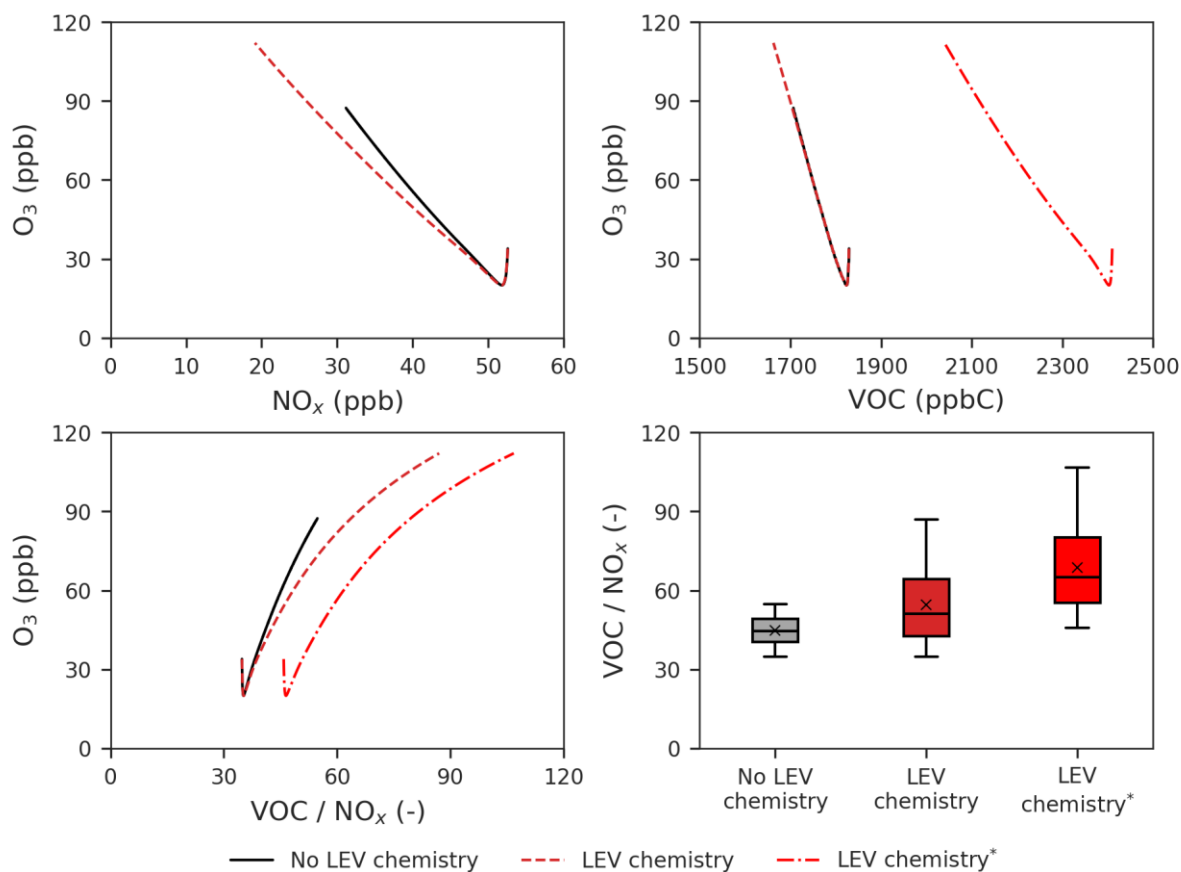


Figure 7 Effects of LEV chemistry on the O₃ versus NO_x, O₃ versus VOC and O₃ versus VOC/NO_x ratio relationships and on the VOC/NO_x ratio. The two cases in red (with LEV chemistry) refer to the two ways in which VOC was determined (with/without LEV_G and LEV_A). The asterisk refers to the inclusion of LEV_G and LEV_A in the total VOC. All the plots show simulation results at the 5-h time scale. Note that findings shown here are determined over a range of F values depending on experimental conditions.

Figures 8-9: Figure 8 (and its caption) was updated based on our response to the “Major comment” and “Suggestion” of reviewer 1 as well as based on revisions suggested by reviewer 2. Related to this figure, Figure 9 is presented here only to show that by using a smaller C_i* (1 μg m⁻³), conditions simulated in Figure 8 also work at α = 1, thus satisfying the Kumala and Wagner (2001) criterion α ≥ 1 discussed in section A. The concentration in the aerosol phase changes slightly in magnitude, particularly in the slowest heterogeneous chemistry scenario (dashed red line), but degradation timescale is not affected in any phase.

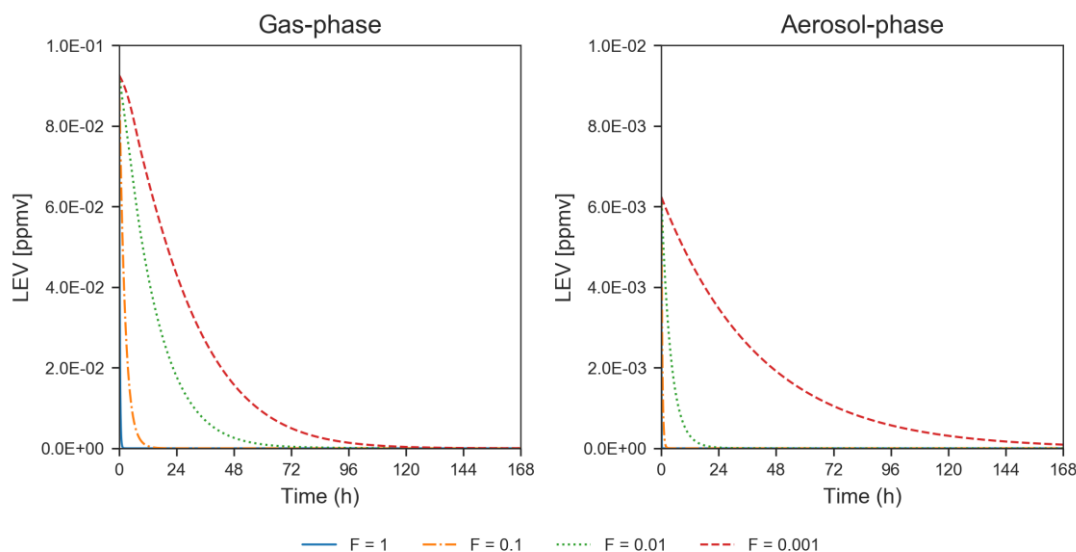


Figure 8 Degradation of LEV by varying the heterogeneous reaction rate coefficient by 4 orders of magnitude, at constant mass accommodation coefficient ($\alpha = 0.1$) and $C_i^* = 13 \mu\text{g m}^{-3}$ (conditions from Hennigan et al. (2010)). Note that the y-axis scale changes between the concentrations presented for the two phases.

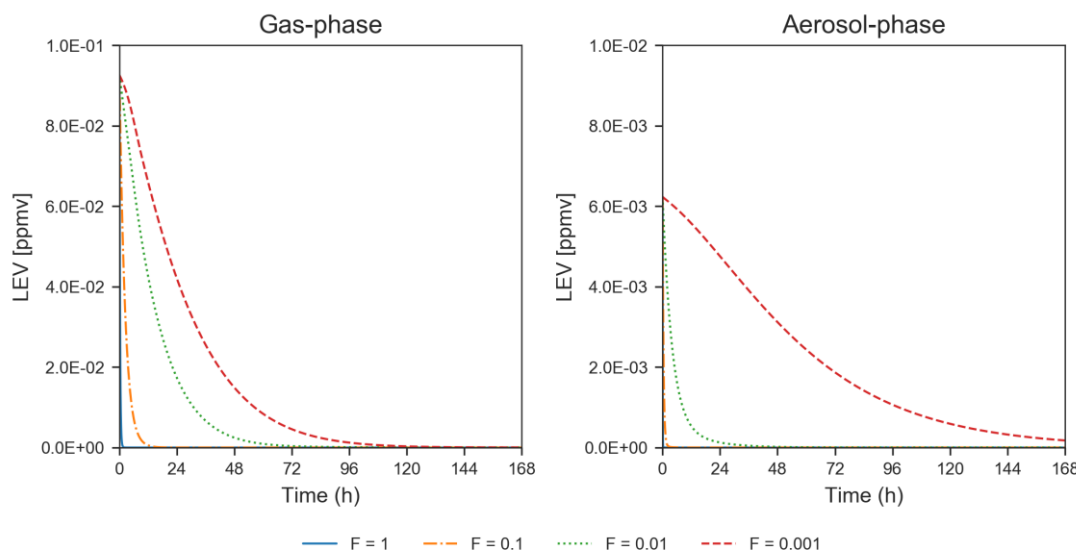


Figure 9 Degradation of LEV by varying the heterogeneous reaction rate coefficient by 4 orders of magnitude, at constant mass accommodation coefficient ($\alpha = 1.0$) and $C_i^* = 1 \mu\text{g m}^{-3}$ (conditions from Hennigan et al. (2010)). Note that the y-axis scale changes between the concentrations presented for the two phases.

Supplemental Information

Revisions of the supplemental information include:

Page revisions

Page 4: We included Pratap et al. (2019) in the citation of experimental conditions used in this study. In addition, we replaced the citation of May et al. (2013) by that of May et al. (2012) for the correct value of C_i^* (298 K).

Reference revisions

We added two new references (see below).

May, A. A., Saleh, R., Hennigan, C. J., Donahue, N. M. and Robinson, A. L.: Volatility of organic molecular markers used for source apportionment analysis: measurements and implications for atmospheric lifetime, *Environ. Sci. Technol.*, 46, 22, 12435-12444, <https://doi.org/10.1021/es302276t>, 2012.

Pratap, V., Bian, Q., Kiran, S. A., Hopke, P. K., Pierce, J. R. and Nakao, S.: Investigation of levoglucosan decay in wood smoke smog-chamber experiments: The importance of aerosol loading, temperature, and vapor wall losses in interpreting results, *Atmos. Environ.*, 199, 224–232, <https://doi.org/10.1016/j.atmosenv.2018.11.020>, 2019.

We corrected some references by adding “and” before the last author.

Figure revisions

Figures S3-S6 have been modified by replacing them with those generated with the new simulations discussed in section A; the new figures are only slightly different, mostly products in the aerosol-phase (LEVP4_A). Figure S7 was added based on results from additional simulations, using conditions from Pratap et al. (2019), and they are consistent with results from Figures S3-S6; however, some differences are obvious, such as the degradation timescale of LEV, timing of product formation and relative importance of products (maybe related to the lowest temperature compared to other cases). The captions of these figures have been modified to show the new α values that were effective after addressing reviewer 1’s comments, respectively 0.1 (Figs. S3-S4) and 0.01 (Figs. S5-S6).

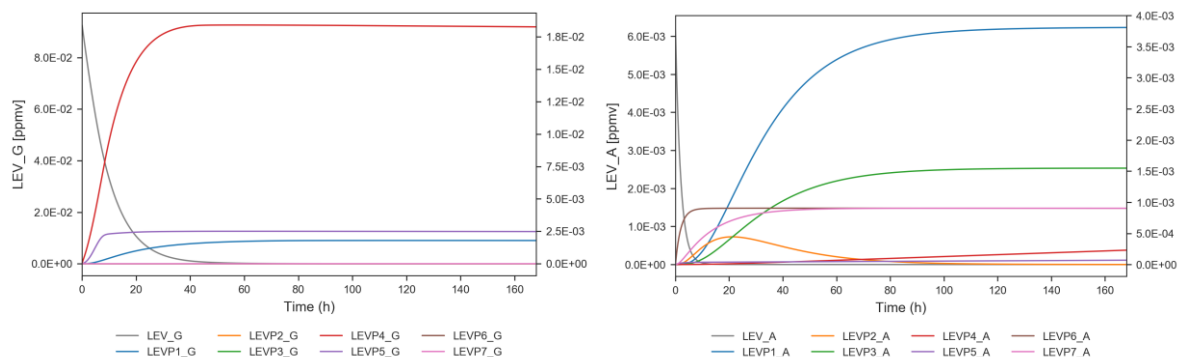


Figure S3: Products of LEV degradation in the gas phase (left) and the aerosol phase (right). ($F = 0.02$; $\alpha = 0.1$) (simulated conditions based on Hennigan et al. (2010)). Concentration of products (ppmv) is displayed on the secondary y-axis.

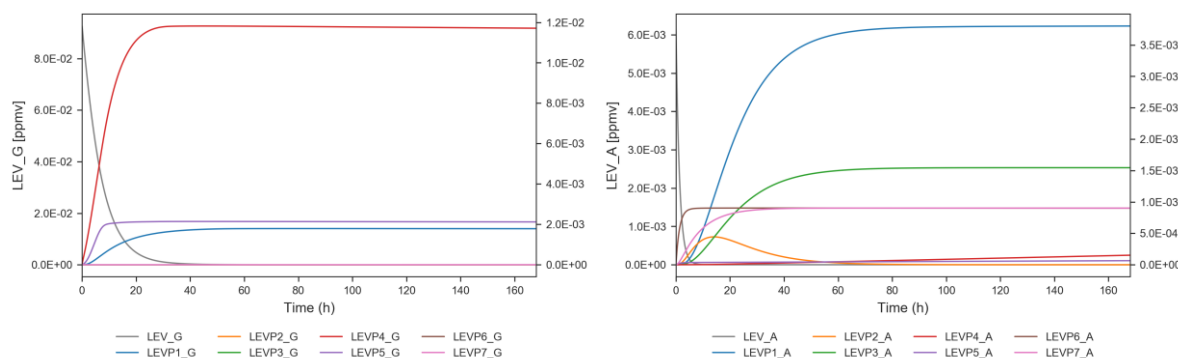


Figure S4: Products of LEV degradation in the gas phase (left) and the aerosol phase (right). ($F = 0.03$; $\alpha = 0.1$) (simulated conditions based on Hennigan et al. (2010)). Concentration of products (ppmv) is displayed on the secondary y-axis.

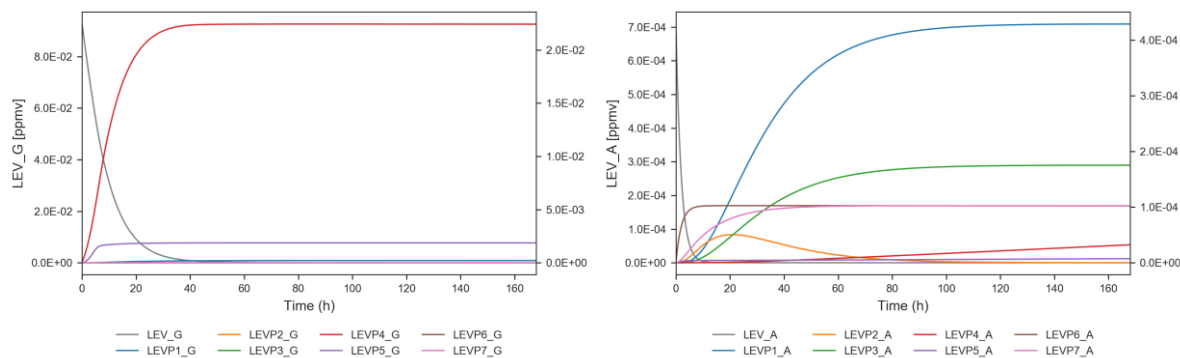


Figure S5: Products of LEV degradation in the gas phase (left) and the aerosol phase (right). ($F = 0.004$; $\alpha = 0.01$) (simulated conditions based on Lai et al. (2014)). Concentration of products (ppmv) is displayed on the secondary y-axis.

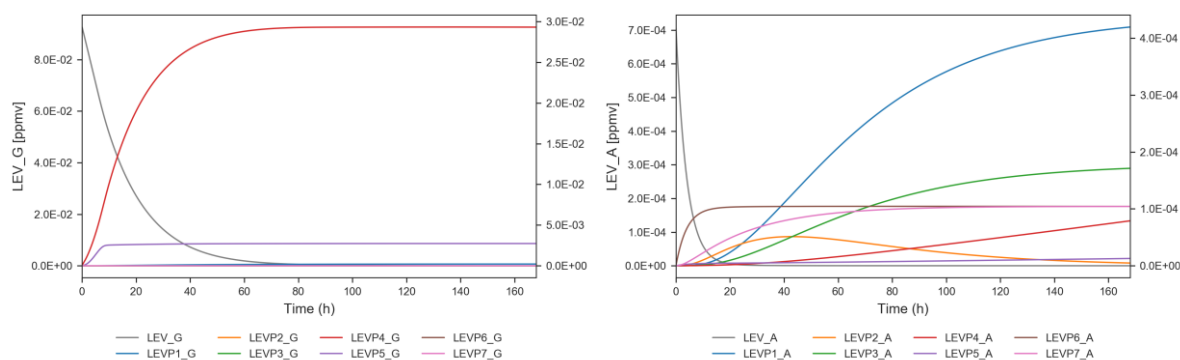


Figure S6: Products of LEV degradation in the gas phase (left) and the aerosol phase (right). ($F = 0.002$; $\alpha = 0.01$) (simulated conditions based on Lai et al. (2014)). Concentration of products (ppmv) is displayed on the secondary y-axis.

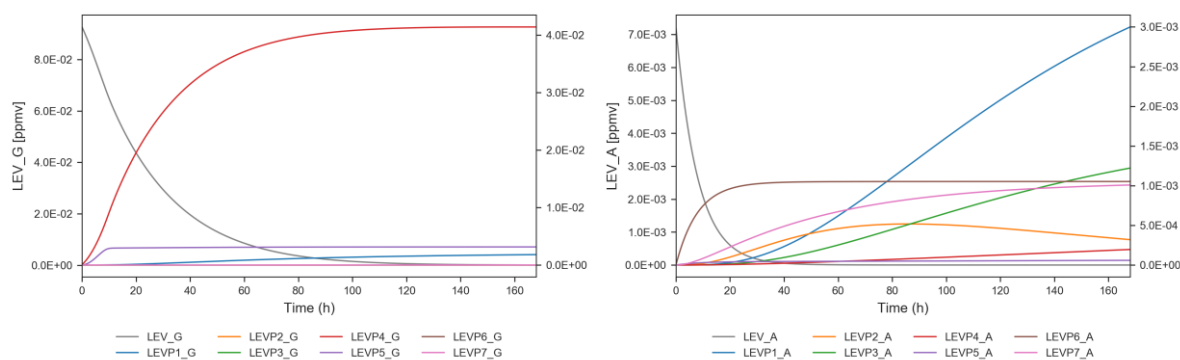


Figure S7: Products of LEV degradation in the gas phase (left) and the aerosol phase (right). ($F = 0.001$; $\alpha = 0.01$) (simulated conditions based on Pratap et al. (2019)). Concentration of products (ppmv) is displayed on the secondary y-axis.

Table revisions

Table S1

We modified this table to include conditions from Pratap et al. (2019), as discussed in section A.

Table S1 Conditions used in chamber simulations for model evaluation

Reference study	LEV_G ₀ (ppmv)*	LEV_A ₀ (ppmv)	H ₂ O (ppmv)	RH (%)	T (K)	D _p (m)	N _t (m ⁻³)	SAD (m ⁻¹)	ΔH _{vap,i} (J mol ⁻¹)	σ (N m ⁻¹)	C _i [*] (298 K) (kg m ⁻³)	ρ (kg m ⁻³)	D (m ² s ⁻¹)
Hennigan et al. (2010)	9.62x10 ⁻²	6.23x10 ⁻³	2.22x 10 ³	10	293.15	5x10 ⁻⁷	3.18x10 ⁷	2.50x10 ⁻⁵	84x10 ³	2.82x10 ⁻²	13x10 ⁻⁹	1.69x10 ³	5x10 ⁻⁶
Lai et al. (2014)	9.62x10 ⁻²	7.09x10 ⁻⁴	1.18x10 ⁴	40	298.15	2x10 ⁻⁷	9.96x10 ⁸	1.25x10 ⁻⁴	84x10 ³	2.82x10 ⁻²	13x10 ⁻⁹	1.69x10 ³	5x10 ⁻⁶
	9.62x10 ⁻²	7.09x10 ⁻⁴	6.60x10 ³	40	288.15	2x10 ⁻⁷	9.96x10 ⁸	1.25x10 ⁻⁴	84x10 ³	2.82x10 ⁻²	13x10 ⁻⁹	1.69x10 ³	5x10 ⁻⁶
Pratap et al. (2019)	9.62x10 ⁻²	7.23x10 ⁻³	3.63x10 ³	30	283.15	2x10 ⁻⁷	9.96x10 ⁸	1.25x10 ⁻⁴	84x10 ³	2.82x10 ⁻²	13x10 ⁻⁹	1.69x10 ³	5x10 ⁻⁶

*The initial gas-phase LEV concentration was determined from its vapor pressure.

A zero-dimensional view of atmospheric degradation of levoglucosan (LEVCHEM_v1) using numerical chamber simulations

5 Loredana G. Suci¹, Robert J. Griffin², Caroline A. Masiello^{1,3}

¹Department of Earth, Environmental and Planetary Sciences, Rice University, Houston, 77005, USA

²Departments of Civil and Environmental Engineering and Chemical and Biomolecular Engineering, Rice University, Houston, 77005, USA

³Departments of Chemistry and Biosciences, Rice University, Houston, 77005, USA

10 *Correspondence to:* Loredana G. Suci (lgs4@rice.edu)

Abstract. Here we developed a zero-dimensional (0-D) modeling framework (LEVCHEM_v1) to provide insights into the atmospheric degradation of -a key tracer emitted during biomass burning - levoglucosan (LEV), while additionally exploring its effects on the dynamics of secondary organic aerosols (SOA) and other gases. For this, we updated existing chemical mechanisms (homogeneous gas-phase chemistry and heterogeneous chemistry) in the BOXMOXv1.7 model to include the
15 chemical degradation of LEV and its intermediary degradation products in both phases (gas and aerosol). In addition, we added a gas-particle partitioning mechanism to the model to account for the effect of evaporation and condensation on the phase-specific concentrations of LEV and its degradation products. Comparison of simulation results with measurements from various chamber experiments ([spanning summer and wintertime conditions](#)) show that the degradation time scale of LEV varied by phase, with [gas-phase](#) degradation occurring over ~1.5-~~3.55~~
20 over ~8-~~24~~-36 hours. These relatively short time scales suggest that most of the initial LEV concentration can be lost chemically or deposited locally before being transported regionally. We varied the heterogeneous reaction rate constant in a sensitivity analysis ([for summer conditions only](#)) and found that longer degradation time scales of LEV are possible, [particularly](#) in the ~~gas phase (5 days) and the~~-aerosol phase (7 days), implying that some LEV may be transported regionally. The multiphase chemical degradation of LEV has effects on SOA and other gases. Several first- or second-generation
25 products resulted from its degradation; most of the products include one or two carbonyl groups, one product contains a nitrate group, and a few products show the cleavage of C-C bonds. The relative importance of the products varies depending on the phase and the timing of the maximum concentration achieved during the simulation. Our estimated secondary organic aerosol SOA yields (~~54~~-32%) reveal that conversion of LEV to secondary products is significant and occurs rapidly in the studied scenarios. LEV degradation affected other gases by increasing the concentrations of radicals and decreasing those of
30 reactive nitrogen species. Decreases of the mixing ratios of nitrogen oxides appear to drive a more rapid increase in ozone compared to changes in volatile organic compounds (~~VOC~~) levels.

An important next step to confirm longer degradation time scales will be to extend the evaluation of the modeled LEV degradation beyond 3-~~5~~-6 hours, by using more extensive data from chambers, and, possibly from fire plumes. The mechanism developed here can be used in chemical transport models applied to fire plumes to trace LEV and its degradation products from source to deposition, assess their atmospheric implications and answer questions relevant to fire tracing, carbon and nitrogen cycling, and climate.

1 Introduction

Knowledge of the atmospheric lifetimes of biomass burning emissions is critical to predict their impacts on photochemistry, air quality and climate. The organic compounds in these emissions are denoted as pyrogenic carbon (PyC) and together they cover a wide range of chemistries and phases, making the determination of individual lifetimes challenging. In the atmosphere, PyC can be in the condensed phase (predominantly as semi- and non-volatile particulate matter, PM) and/or in the gas phase (volatiles). Both phases participate in atmospheric photochemistry. For instance, volatile organic compounds (VOC) react with hydroxyl radical (OH) and contribute to tropospheric ozone (O₃) formation. Other gases released during biomass burning, such as polycyclic aromatic hydrocarbons, can be oxidized, the products of which may form semi- or non-volatile PM. Both directly emitted and secondarily formed PM alters visibility (through light extinction), human health (through respiration) and climate forcing (via absorption/scattering of solar radiation). Depending on its chemical and physical properties, PM also participates in cloud formation as cloud condensation nuclei and influences the physics and chemistry of clouds. Through alterations of physical properties of clouds, PM indirectly contributes to climate forcing. The magnitude and the extent of PyC impacts depend on its atmospheric lifetime.

Anhydrosugars, the most abundant of which is levoglucosan (LEV), are molecular tracers of PyC that traditionally have been used as markers for biomass burning in ambient aerosols, or as markers for wildfires in sediments and ice cores (Suciu et al., 2019 and references therein). However, their degradation and lifetimes are not well understood in any environment, including the atmosphere and cryosphere, two environments that are related via atmospheric transport and deposition of such PyC tracers. Therefore, understanding the atmospheric fate of anhydrosugars is essential not only to understanding fire effects on air quality but also to interpreting fire records in ice, and to studying the complex relationship between fire, vegetation and climate.

Experimental laboratory studies (in chambers or flow tubes) on LEV chemical degradation suggest that its atmospheric lifetimes vary widely, from minutes to months (Hennigan et al., 2010; Hoffman et al., 2010; Kessler et al., 2010; Knopf et al., 2011; Bai et al., 2013; Lai et al., 2014; Slade and Knopf, 2014; Arangio et al., 2015; Gensch et al., 2018; [Pratap et al., 2019](#)). In addition, the multiphase ~~character~~-chemistry of LEV and its gas-particle partitioning (G/P) between phases has not been explicitly considered yet in laboratory studies of its chemical kinetics. Given its semi-volatile nature, the evaporation/condensation effect in conjunction with chemical kinetics must be given attention in the estimation of LEV lifetimes, especially those with respect to chemical degradation. Some models, such as the non-equilibrium kinetic

evaporation model of May et al. (2013) consider this. Previous studies applied the gas-particle partitioning model of May et al. (2013) to levoglucosan but its multiphase chemical decay was limited to the reaction with the OH radical only (Pratap et al., 2018; 2019).

To estimate more accurately the atmospheric degradation time scales (modelled decay of concentration over time relative to initial concentration), anhydrosugar chemistry must be studied in more complex atmospheric settings than those reproduced in the laboratory. This could be achieved using three-dimensional (3-D) chemical transport models (CTMs). However, current CTMs do not treat anhydrosugars individually in their chemical mechanisms. This is partly because these models often are motivated by the need to quantify only PM mass to meet air quality legislation. Thus, studies often report modeled species such as PM_{2.5} (that with diameters smaller than 2.5 microns), organic carbon in PM (OC), and black carbon (BC) (In et al., 2007; Alvarado et al., 2009; Simon and Bhave, 2012; Pye and Pouliot, 2012; Heron-Thorpe et al., 2014; Alvarado et al., 2015). Moreover, because anhydrosugars are also semi-volatile they participate in both gas- and aerosol-phase chemistries, so placing them into just one single category (i.e., PM_{2.5}) is inaccurate. In general, individual emissions from biomass burning are lumped into categories, assuming that all species behave identically with respect to chemical and physical transformation or loss. While this assumption eases the computational burden of the chemistry and physics of the model, it can yield inaccurate results regarding the modeled species; it also does not allow the study of tracers individually.

Here we developed ~~use~~ a zero-dimensional (0-D) modeling framework (LEV_{CHEM_v1}) to study the chemical degradation of LEV. Because the two isomers of LEV (mannosan and galactosan) have similar structures but different arrangements of the hydroxyl groups, this study only focuses on chemical reactions involving LEV. A future goal is to expand LEV_{CHEM_v1} to include the degradation of the two isomers and, then, to implement the full mechanism of anhydrosugar degradation into 3-D CTMs. The 0-D modeling approach here can identify model uncertainty attributable to the mechanism only; when the mechanism is used in a CTM, other sources of uncertainties (advection, diffusion, deposition, etc.) in the overall uncertainty of the model predictions can be assessed.

Several research topics pertinent to the chemical degradation of LEV are dealt with in this study. These will be addressed after a discussion of the model framework and development.

First, we explore the degradation time scale of LEV, and what can be inferred ~~from~~ from it regarding the scale of its impact (local versus regional). For example, isolating the effect of chemistry from transport or other physical processes may yield different degradation time scales, resulting in different inferred transport distances, impacting whether local- or regional-scale chemistry may be the dominant process controlling the lifetime of LEV.

Second, we examine the contribution of LEV degradation to the formation of secondary organic aerosols (SOA), including changes in total PM mass and the relative importance of degradation products. Significant LEV degradation may lead to higher SOA yields. This information can further be used as a reference to understand SOA formation in a 3-D CTM framework.

Third, we examine how LEV degradation affects the concentrations of other gases such as O₃ and its precursors, nitrogen oxides (NO_x = nitric oxide (NO) + nitrogen dioxide (NO₂)) and VOC, total reactive nitrogen (NO_y) and NO_x oxidation

products ($\text{NO}_z = \text{NO}_y - \text{NO}_x$). Considering its multiphase chemistry that also generates peroxy radicals (RO_2), LEV may have an important effect on these pollutants.

100 2 Modeling approach

2.1 Overview of the 0-D modeling framework and mechanisms

The 0-D model used to develop LEVCHEM_v1 in this study (BOXMOX v1.7) (Knote et al., 2015) is a publicly available software that expands on earlier code, the Kinetic Pre-Processor (KPP v2.1) (Sandu and Sander, 2006). The two models are briefly described below.

105 The KPP generates code using chemical reactions and their respective reaction rate coefficients as inputs (Sandu and Sander, 2006). The rate of change in concentration of a species i ($\frac{dC_i}{dt}$) is expressed as the difference between its production (P) and loss (L) rates (eq. 1).

$$\frac{dC_i}{dt} = P - L \quad (1)$$

The generated code (which determines the P and L terms in eq. 1) then is used in a temporal integration to compute the
110 change in concentration of the individual reactants and products based on a system of ordinary differential equations (ODE). The KPP offers a variety of stiff numerical integrators that can be selected by the user in order to maximize the computational efficiency of the ODE system within a low to medium accuracy regime (Sandu and Sander, 2006).

The BOXMOX extends the KPP capabilities even further by providing a framework in which various numerical experiments are possible, such as chamber experiments or boundary layer atmospheric chemistry numerical experiments (Knote et al.,
115 2015). These are possible with the addition of a wrapper to the KPP. The wrapper allows the user to add inputs to the model, such as initial conditions, environmental conditions, boundary conditions, time-varying photolysis rates, turbulent mixing, emissions, deposition, etc., in order to run numerical experiments; it also allows the user to add new code to further develop the model. The model outputs time series of species concentrations, rate constants and other user-specified [outputs information](#).

120 2.2 Mechanistic development

We integrated the multiphase chemical degradation of LEV into BOXMOXv1.7 by adding chemical reactions along with their reaction rate coefficients to existing homogeneous gas-phase and heterogeneous mechanisms (LEVCHEM_v1). These existing mechanisms already have been implemented and tested by the BOXMOXv1.7 developers (Knote et al., 2015).

Based on its similarity to mechanisms used in 3-D CTMs, we chose the Carbon Bond version 2005 with Toluene Updated
125 Chlorine Chemistry as the homogeneous gas-phase mechanism to implement the gas-phase degradation of LEV. This was recently updated by the U.S. EPA to include additional tropospheric chemistry (CB05TUC1_EPA). It contains 148 chemical reactions that constitute the core of the mechanism or the “CB05” part (Yarwood et al., 2005; Whitten et al., 2010), 23

reactions for the reactive chlorine chemistry or the “TUCI” part, 10 reactions for formation of secondary aerosols from gas-gas reactions, and 24 photolysis reactions (Knote et al., 2015). In total, the overall gas-phase mechanism included 205
 130 reactions and 82 variable species to describe gas-phase tropospheric photochemistry. Here we extended the CB05TUCI_EPA mechanism to include 13 reactions and 10 species (radicals and 1st or 2nd generation products) associated with LEV chemistry in the gas phase (see Table 1). (Chemical structures are shown in Figure S1 and Figure S2 in the Supplemental Information). Thus, the total number of reactions and species in the updated gas-phase mechanism increased to 218 and 99, respectively.

135 The homogeneous gas-phase reaction rate coefficients (Table 1) were modeled as constants (when available in the literature) or as Arrhenius type reaction rate coefficients (eq. 2) using functions developed previously (Knote et al., 2015) with measured, assumed or calculated parameters:

$$k = A * \exp\left(\frac{-E}{RT}\right) \quad (2)$$

where k is the homogeneous second-order gas-phase reaction rate coefficient ($\text{cm}^3 \text{ molecules}^{-1} \text{ s}^{-1}$), A is the collision frequency factor ($\text{cm}^3 \text{ molecules}^{-1} \text{ s}^{-1}$), E is the energy barrier for the reaction (kJ mol^{-1}), R is the ideal gas law constant ($8.314 \text{ J mol}^{-1} \text{ K}^{-1}$) and T is temperature (K).
 140

When the collision rate coefficient A was not available in the literature, we calculated it using eq. 3 (Seinfeld and Pandis, 2006) applied to two spherical bodies (molecules) A and B:

$$A = \pi d^2 \sqrt{\left(\frac{8k_B T}{\pi \mu}\right)} \quad (3)$$

145 where d^2 represents the squared sum of the two radii of A and B (m^2) while the term under the square root is the relative velocity of the A and B collision bodies in which k_B is the Boltzmann constant ($1.381 \times 10^{-23} \text{ J K}^{-1}$) and μ is the reduced mass (eq. 4):

$$\mu = \frac{m_A * m_B}{(m_A + m_B)} \quad (4)$$

The heterogeneous chemical mechanism HETCHEM was developed by Knote et al. (2015) to model the heterogeneous
 150 interaction between dinitrogen pentoxide (N_2O_5) and water bound to solid aerosols or PM. The heterogeneous reaction rate ($k_{\text{SFC_REACTION}}$) was modeled by Knote et al. (2015) based on first-order surface uptake from Fuchs and Sutugin (1971) (eq. 5):

$$k_{\text{SFC_REACTION}} = \frac{1}{4} * \gamma * \omega * \text{SAD} \quad (5)$$

where γ represents the uptake coefficient of the gas-phase oxidant species i (ranging from 0 to 1), ω is the mean molecular
 155 velocity (m s^{-1}) and SAD is the aerosol surface area ~~or surface area~~ density ($\text{m}^2 \text{ m}^{-3}$). The mean molecular velocity is calculated via eq. 6:

$$\omega = 1.455 * 10^2 * \sqrt{\frac{T}{MW * 10^3}} \quad (6)$$

where T is the temperature (K) and MW is the molecular weight of the gas species (kg mol^{-1}).

Using the same expression for the heterogeneous reaction rate as in eq. 5, we implemented the heterogeneous chemistry of
 160 LEV in the form of 1st order reactions (see Table 2) and using uptake coefficients (γ) available from literature (experimental
 measurements) or calculated in this study based on the collision theory (Seinfeld and Pandis, 2006), thermodynamic
 parameters from Bai et al. (2013), and the relationship between γ and the second-order heterogeneous reaction rate constant
 for the reaction of LEV with the OH radical (Kessler et al., 2010). When the uptake coefficient was not available in the
 literature, eq. 7 was used to calculate the uptake coefficient for the heterogeneous reaction of particle-phase LEV (and its
 165 degradation products):

$$\gamma_{i,OH} = \frac{2D_0\rho_i N_A}{3\bar{c}_{OH}M_i} k_{i,OH} \quad (7)$$

where $\gamma_{i,OH}$ is the effective gas-phase oxidant uptake coefficient by species i (here, the gas-phase oxidant being OH), D_0 is
 the surface-weighted average diameter of the particle at the beginning of the experiment (in this study, the particle diameter
 was assumed to be constant throughout the simulations and is denoted as D_p), ρ_i is the density of the organic species, N_A is
 170 Avogadro's number (6.022×10^{23} molecules mol⁻¹), \bar{c}_{OH} represents the average velocity of the gas-phase OH radical (or
 other oxidant), M_i is the molecular weight of the organic species and $k_{i,OH}$ is the second-order heterogeneous reaction rate
 constant. This study used an average of several heterogeneous reaction rate constants (2.85×10^{-13} cm³ molec⁻¹ s⁻¹) measured
 by Slade and Knopf (2014). We assumed this value for all LEV degradation products (including for the radical LEVROOH,
 see reaction 9 in Table 2) due to the fact that experimental heterogeneous reaction rate coefficients have not been measured
 175 for LEV products.

The G/P mechanism used in this study (as part of LEVCHEM_v1) was taken from May et al. (2013) and describes the rate
 of change in concentration of both gas-phase and particle-phase species due to evaporation and condensation (eq. 8 and 9).

$$\frac{dC_{p,i}}{dt} = -CS(X_{m,i}Ke_iC_i^* - C_{g,i}) \quad (8)$$

$$\frac{dC_{g,i}}{dt} = -\frac{dC_{p,i}}{dt} \quad (9)$$

180 Changes in the particle-phase concentration ($C_{p,i}$) are tracked simultaneously based on the difference between the gas-phase
 concentration of species i ($C_{g,i}$) and the theoretical surface equilibrium concentration (C_i^*) (eq. 10), corrected for the mass
 fraction of species i in the particle phase ($X_{m,i}$) (eq. 11) and the Kelvin effect (Ke_i) (eq. 12):

$$C_i^*(T) = C_i^*(298\text{ K}) \exp \left[-\frac{\Delta H_{vap,i}}{R} \left(\frac{1}{T} - \frac{1}{298\text{ K}} \right) \right] \frac{298\text{ K}}{T} \quad (10)$$

where $C_i^*(298\text{ K})$ represents the saturation concentration of species i at 298 K and $\Delta H_{vap,i}$ is the enthalpy of vaporization of
 185 species i . From a mass balance, the changes in the two concentrations are equal but opposite in sign.

$$X_{m,i} = \frac{f_i C_{tot}}{C_{OA}} \left(1 + \frac{C_i^*(T)}{C_{OA}} \right)^{-1} \quad (11)$$

where f_i represents the mass fraction of the organic species i , C_{tot} is the total concentration of the organics (gas and aerosol
 phases) and C_{OA} is the total concentration of organic aerosols.

$$Ke = \frac{4\sigma MW_i}{\rho RT D_p} \quad (12)$$

190 where σ represent the surface tension of the bulk particle, MW_i is the molecular weight of the organic species i , ρ is the bulk density of the particle and D_p is the particle diameter.

The first order condensation sink (CS) (eq. 13) is a function of D_p , total particle number concentration (N_t), the diffusion coefficient of the organic vapor in air (D) and the Fuchs-Sutugin correction factor (C_{F-S}) that accounts for effects of non-continuity (eq. 14).

$$195 \quad CS = 2\pi D_p N_t D C_{F-S} \quad (13)$$

The C_{F-S} depends on the Knudsen number (Kn) and the mass accommodation coefficient (α).

$$C_{F-S} = \frac{1+Kn}{1+0.3773Kn+1.33Kn\frac{1+Kn}{\alpha}} \quad (14)$$

The dimensionless Knudsen number (eq. 15) is defined as the ratio between the mean free path of organic molecules in air ($\lambda = 62.5$ nm) and the particle radius ($D_p/2$).

$$200 \quad Kn = 2 \frac{\lambda}{D_p} \quad (15)$$

The mass accommodation coefficient represents the probability of a vapor sticking to the particle surface once a collision occurs; numerically, α ranges from 0 (no accommodation) to 1 (perfect accommodation) (Seinfeld and Pandis, 2006).

2.3 Simulations and sensitivity analysis

For both model evaluation and sensitivity, we ran multiple 7-day simulations at 10-second temporal resolution in various scenarios, from fast (the default case) to relatively slower heterogeneous chemistry. The heterogeneous chemistry was varied to account for other controls on LEV concentration that were not explicitly considered in the present 0-D modeling approach, such as aerosol matrix effects (composition, mixing state, multilayer kinetics, liquid water content, etc.). These additional controls were lumped into a single factor (F) which, for model evaluation, was assumed to vary according to the conditions in chamber experiments. We expect F to be, at a maximum, 0.1 due to observed mass fractions in biomass burning organic aerosols (Sullivan et al., 2014). However, for sensitivity analysis, we varied F from 1.0 (default case) to lower values (0.1, 0.01 and 0.001) to slow down the heterogeneous reaction rates. In addition, we varied the mass accommodation coefficient (see eq. 14) from a default case of (which is 0.1 (which is the lower limit of α for a system in equilibrium (May et al., 2013)) to lower values (0.01 and 0.001) and larger values (1.0). It was necessary to vary α because its value is unknown for levoglucosan and its degradation products. The mass accommodation coefficient is related to the G/P partitioning mechanism (eq. 14)– and the uptake coefficient (γ). Theoretically, $\alpha \geq \gamma$, depending on the Knudsen number (Kulmala and Wagner, 2001).

The initial conditions of aerosol-phase LEV represent the average of initial concentrations used in chamber experiments (Hennigan et al., 2010; Lai et al., 2014; Pratap et al., 2019) (Table S1 in the Supplemental Information). The initial LEV concentration in the gas phase was set to its vapor pressure in all the scenarios (Table S1). We estimated the initial conditions of other species in the chemical mechanism as well as photolysis rate constants by running 1-h resolution of daily

3-D CTM simulations (Community Multi-scale Air Quality Model, CMAQv5.0.2) using inputs (emissions and meteorology) from Rasool et al. (2016). These conditions correspond to the location, altitude, and timing of a small prescribed-fire plume in South Carolina (Sullivan et al., 2014).

For ~~one~~-aerosol property (D_p), air temperature, pressure and relative humidity values, we used values from chamber experiments (Hennigan et al., 2010; Lai et al., 2014; [Pratap et al., 2019](#)) (Table S1). Other parameters (N_b , SAD , $\Delta H_{vap,i}$, σ , C_i^* (298 K) and ρ) that were not measured in chamber experiments but were used in simulations are also given in Table S1.

3 Results and discussion

3.1 Model evaluation

We evaluated the model (LEVCHEM_v1) by comparing simulation outputs (i.e. concentration) with experimental chamber data in scenarios in which simulations were initialized using chamber conditions. In particular, we investigated the contributions of LEV degradation to SOA, the change in total PM mass and the effects on other gases like O₃ and NO_x. We also examined the sensitivity of the degradation time scale of LEV and SOA yields to model parameters.

We evaluated the two-phase (gas-aerosol) modeling of LEV degradation by comparing the time-series of aerosol LEV concentration resulting from simulations to those obtained from laboratory chamber experiments (only the particle phase data) over 5–6 hours (Figure 1). Overall, the model predicted that LEV degradation closely follows the measured LEV degradation in relatively slower heterogeneous chemistry scenarios ($F = 0.001, 0.002; 0.004; 0.02; 0.03$, depending on the experimental data considered) and at ~~low~~-mass accommodation coefficients of 0.1 and 0.01(0.001). These α values are smaller than those of γ for most of the chemical species, including for levoglucosan. However, as seen in Table 2, the great majority of the γ values were computed in this study, in the absence of their experimental measurements. In eq. 7, we assume a similar 2nd order heterogeneous reaction rate for all the species; this may bias our calculations of γ towards larger values. For γ values on the order of 10^{-1} (OH uptake by levoglucosan, for example) and Knudsen numbers on the order of 10^{-1} (all modeled cases), the corresponding α should be ~ 0.1 , according to Fig. 1 in Kulmala and Wagner (2001). This is true when we model conditions from Hennigan et al. (2010); thus, in this case the $\alpha \geq \gamma$ criterion is marginally satisfied. Modeled conditions from Lai et al. (2014) and Pratap et al. (2019) do not meet this criterion for levoglucosan because, for similar Kn and γ values, the model worked well (compared to experimental data) only at $\alpha = 0.01$; in these cases, $\alpha < \gamma$. However, for other species with smaller γ (O₃ and N₂O₅), all the modeled cases in our study satisfy the criterion $\alpha \geq \gamma$. It is worth noting here that the effective α values we found in our study by comparing model predictions with data have inherent uncertainties associated with both the data and the model. The one order of magnitude difference between F values may be explained by the different initial LEV concentration used in both experiments and simulations (which is one order of magnitude as well) and, to a smaller extent, by the differences in relative humidity (Table S1). For instance, Hennigan et al. (2010) used drier conditions in chamber experiments compared to Lai et al. (2014) and Pratap et al. (2019). However, the model does not

capture fast degradation in one case (red dots) in the first hour of simulation and the plateau observed after three hours (diamonds and triangles). While the first case may be explained by the uncertainty in the modeled heterogeneous reaction rate that is varied by F, the second case could be explained by the fact that, in chamber experiments, the build-up of matter at the surface of the aerosol prevents LEV in the aerosol reacting with gases or partitioning to the gas phase. The scattering in the chamber data relative to model lines could also be explained by the different source of LEV used in chamber experiments compared to the model (wood smoke particles and smoke extract versus pure LEV particles).

One-to-one comparison of predicted versus measured LEV degradation (Figure 2) from all the simulated scenarios (red, blue and bluegreen) shows that the model performs very well for some of the data points (those that fall within the $\pm 30\%$ limits) but the average absolute error of the model is relatively large (4847%). Overall, the model underpredicts the LEV concentration (average relative error of -4847%). The linear agreement between the model predictions and the experimental data is strong (coefficient of determination of 0.78).

While only the first five-5-6 hours of the simulations could be evaluated using chamber measurements, the simulated LEV degradation continued after this length of time until LEV concentration was nearly zero, 1.5-3.5 days in the gas phase and 8-24-36 hours in the aerosol phase (Figure 3). These longer time scales are a first estimate of degradation time scales of LEV.

The relative importance of degradation products differs in the two phases (see Table 1 and Table 2 for processes leading to formation of these products; also see Figure S1 and Figure S2 in the Supplemental Information for chemical structures), with LEVP4 and LEVP5 dominating the gas phase and LEVP6, LEVP7 and LEVP2 dominating the aerosol phase over the first 5-6 hours (Figure S3 to Figure S4-S7 in Supplemental Information). LEVP4 is a product formed only by the gas-phase chemistry (reaction 6 in Table 1) and contains a carbonyl group after this reaction (Figure S1 in Supplemental Information). LEVP5 is a nitrated organic (Figure S1 in Supplemental Information) that is theoretically generated by both chemical mechanisms (reaction 13 in Table 1 and reaction 14 in Table 2). Products LEVP6 and LEVP7 (Figure S1 in Supplemental Information) are results of the fragmentation pathway specific only to heterogeneous chemistry (reactions 10-11 in Table 2); they both contain a carbonyl group (Figure S1 in Supplemental Information). LEVP2 is a product of reaction 4 (Table 1) and reaction 5 (Table 2); it contains two additional functional groups compared to LEV: a carbonyl and an ether (Figure S1 in Supplemental Information). The relative importance of products slightly changes beyond 5-6 hours, particularly in the aerosol phase, in which LEVP3 becomes more important than LEVP2. LEVP3 is the largest molecular product (Figure S1 in Supplemental Information) that is generated by the multiphase LEV chemistry in reactions 5 (Table 1) and 6 (Table 2). Through subsequent reactions, LEVP3 can grow into a larger molecule that would ultimately contribute to the nucleation of new PM (Bai et al., 2013).

~~Decreasing the rate of heterogeneous chemistry by one order of magnitude has little effect on the relative importance of products (Figure S5 to Figure S6 in Supplemental Information). While this shifts the timing of the maximum concentration in both phases, it has a more important effect on concentration of the product, becoming lower in the aerosol phase and higher in the gas phase, suggesting that evaporation dominates over heterogeneous chemistry. The concentrations of~~

285 ~~products in the aerosol phase are all drivers of SOA yields; it is thus important to know the main molecular SOA composition resulting from LEV degradation and G/P partitioning.~~

3.2 Contribution of levoglucosan degradation to SOA

Traditionally, reactant organic species in the gas phase are considered to contribute to new SOA formation (or new SOA mass). However, in this study, since LEV is present in both phases and its chemistry generates products in both phases that
290 can partition from one phase to another, both LEV_G (gas) and LEV_A (aerosol) can be treated as SOA precursors. Thus, they are both included in SOA yield calculation. Using eq. 16, the SOA yield is calculated as the ratio between the mass of SOA formed and the mass of the reacted precursors (Stefenelli et al., 2019).

$$SOA\ yield\ (\%) = \frac{\sum_{i=1}^n LEV_{Pi-A}}{(LEV_{G_0} + LEV_{A_0}) - (LEV_G + LEV_A)} \quad (16)$$

where **LEV_{Pi-A}** represents a LEV oxidation product in the aerosol phase, subscript “0” refers to initial conditions and $n =$
295 7. The terms represent mass concentrations. Formation of SOA from LEV degradation occurs rapidly (in the first ~~12-12-34~~ minutes of the simulation), with maximum SOA yields ranging from ~~5-4~~ to 32% (Figure 4a). These high SOA yields in the first 6 hours are the result of rapid conversion of the precursors to aerosol-phase products, mainly due to heterogeneous chemistry. Because these products are not seen in the gas phase, evaporation does not influence the SOA yields in this early stage of the simulation; condensation of gas-phase products (LEVP4 and LEVP5) is also negligible (see Fig. S3-S7). Most of
300 the oxidation products remain in the aerosol phase over the entire simulation period, except for LEVP5 and LEVP1 that may partition to the gas phase. SOA yield reaches steady-state at ~24-26 hours due to near-zero concentrations of the two precursors and the presence of oxidation products from heterogeneous chemistry and G/P partitioning (i.e., condensation of LEVP4) in the aerosol phase. Among the simulated scenarios, the largest SOA yields resulted from slightly faster heterogeneous chemistry scenarios (by one order of magnitude), initialized with when higher initial LEV_A concentrations
305 (by one order of magnitude) and occurring on larger particles (larger diameter by a factor of two) were used in the simulations and they did not decrease below 8% in wintertime conditions (Figure 4a and Table S1). The heterogeneous chemistry was the slowest for SOA yields predicted for winter conditions (suggested by $F = 0.001$) while it was the fastest for those associated with summer conditions ($F = 0.02-0.03$). The total aerosol mass (the sum of concentrations of all LEV-related aerosol species, including the radicals) also increased by ~~14-8-15%~~ in the first ~~six hours minutes~~ and kept increasing,
310 although at a slower pace, to up to 18-29% at the end of remained constant throughout the simulation period. The smallest total aerosol mass in the first six hours (8%) was observed in modeled wintertime conditions, while the highest total aerosol mass (14-15%) was observed in summertime conditions. This-These suggests that the multiphase chemistry of LEV along with its phase partitioning cannot be ignored in assessments of fire air quality effects and can have variable effects on SOA yields depending on the initial conditions and aerosol properties.

315 3.3 Effects of LEV degradation on other gases

Implementation of LEV chemistry in models can also be used to consider its effects on other atmospheric species to better understand the effects of fire on air quality and atmospheric chemistry, such as the formation of tropospheric O₃ in the presence of NO_x and VOC (both emitted from fires), conversion of NO_x to other reactive nitrogen forms (including nitrated LEV), interaction with key gas-phase species oxidants, etc. We studied effects in the model scenarios by comparing the concentrations of those key species obtained with LEV chemistry and those obtained without LEV chemistry (Figure 5 and Figure 6).

We found that LEV chemistry including G/P partitioning on average increases the concentrations of OH, nitrate radical (NO₃), O₃, nitric acid (HNO₃) and NO_z, while it decreases the concentrations of N₂O₅, NO_x and total VOC (that does not include LEV_G and LEV_A). These effects are the net result of full LEV chemistry in which species may be consumed or generated. For example, OH is consumed in reactions 1 and 10 but it is also generated directly in reactions 4 and 12, and indirectly through its precursor HO₂ that is generated by reactions 3, 6 and 12 (Table 1).

LEV chemistry modulates the concentration of reactive species that also interact with other VOC. Because LEV chemistry increases the concentrations of key oxidants (OH, NO₃, O₃), it causes the concentration of total VOC to decrease over time due to increased availability of their oxidants. LEV chemistry also causes NO_z to increase over time; this can mainly be explained by the formation of nitrated organic compounds (LEVP5_G and LEVP5_A) and HNO₃ in reactions 13 (Table 1) and 14 (Table 2). LEV chemistry also generates NO₃ precursors (such as NO₂) that may explain the net increase in NO₃ concentration (Figure 5).

We also studied the effects of LEV chemistry on the O₃ versus NO_x, O₃ versus VOC and O₃ versus VOC/NO_x ratio relationships as well as effects on the VOC/NO_x ratio itself (Figure 7). While the decay of NO_x slowed down the increase of O₃, the decay of VOC had no effect on the rate of O₃ formation when total VOC did not contain LEV_G and LEV_A. When the latter two were included in total VOC, the decay of total VOC also reduced the rate of the O₃ increase (linear slope of $-0.24190.250 \pm 0.001$ ppb/ppbC) but not as much as NO_x did (linear slope of -0.288 ± 0.008 ~~-2.821 ± 0.007~~ ppb/ppb). The VOC/NO_x ratio increases when LEV chemistry is considered, driving O₃ to reach higher concentrations (~~$+17$~~ -112 ppb) compared to the default case (without LEV chemistry). Thus, when LEV chemistry operates in the system, the change in O₃ concentration is primarily driven by the change in NO_x and only secondarily by the change in VOC.

3.4. Sensitivity analysis

Heterogeneous chemistry is the most sensitive aspect of the modelling approach in the present study. Here we assumed that the aerosol surface is composed of pure LEV and there are many factors that can interfere or inhibit heterogeneous chemistry of a pure LEV substrate (section 2.3). These controls were lumped into a single factor (F) that we varied from a default case (1.0) to cases in which heterogeneous chemistry was up to three orders of magnitude slower. While available chamber experiments studies offered the opportunity to evaluate LEV degradation for a given heterogeneous reaction rate coefficient

that was reduced by certain F values (see section 3.1), other values of F are plausible. As a starting point, here we show how these F values influence the degradation time scale of LEV (Figure 8) and the SOA yields (Figure 4b). Within this wide range of heterogeneous reactions rates (at constant $\alpha = 0.001$), the degradation time scale of LEV can be as long as 5 days in the gas phase and 7 days in the aerosol phase (when $F = 0.001$). While the time scale of gas-phase LEV is similar (5 days) to that ~~These are larger time scales than those~~ observed with reaction rates used in chamber comparisons (see section 3.1), the time scale of aerosol-phase LEV is much larger (7 days versus 36 hours), suggesting and suggest that LEV associated with PM can be transported and deposited ~~both locally and~~ regionally. Over these time scales, SOA yields vary roughly within the same range (~~714-3233~~%) as observed in the previous cases considered (see section 3.2). ~~Compared to model scenarios evaluated by chamber experiments (Figure 4a), the SOA yields start levelling out only after 4-5 days as opposed to 1 day, suggesting that some SOA still forms in the one to four to five day window.~~

We also tested the sensitivity of the mass accommodation coefficient (α) at $F = 0.01$, using conditions from Hennigan et al. (2010). Varying ~~this~~ α by four orders of magnitude (0.001, 0.01, 0.1 and 1.0) showed little effect on LEV degradation (i.e., degradation in the gas phase was slightly faster when $\alpha = 1$, while degradation in the aerosol phase was slightly faster when $\alpha = 0.001-0.1$) in comparison to the effect of slowing down the heterogeneous chemistry (F, as described above). The effect of the mass accommodation coefficient on LEV degradation appears to be more important when the G/P partitioning is modelled as gas-aerosol equilibrium reactions of which the partitioning coefficient is modelled with eq. 13. This is a different way to implement the G/P partitioning in the model, but it does not drive species phase transfer based on the theoretical surface equilibrium concentration (eq. 8 and 9).

4 Conclusions

Anhydrosugars emitted by biomass burning are key tracers of PyC and of carbon cycling throughout Earth system reservoirs. However, relatively little is known about their degradation in any environment. A better understanding of the atmospheric degradation of anhydrosugars is necessary for both atmospheric and cryospheric sciences because it will improve the understanding of air quality effects of fire as well as the interpretation of levoglucosan records of fire, paleoclimate and paleovegetation recorded in the ice (Gambaro et al., 2008; Kawamura et al., 2012; Kehrwald et al., 2012; You and Xu, 2018). This study focused on the atmospheric degradation of anhydrosugars from the perspective of LEV, the most abundant anhydrosugar emitted on a mass basis.

Using a 0-D modeling framework (BOXMOXv1.7), we implemented multiphase chemistry and G/P partitioning of LEV and its initial oxidation products (LEVCHEM_v1). We found that LEV degradation time scale ranges from ~~8-21-8-36~~ hours (aerosol-phase) to ~~4.5-3.5-1.5-5~~ days (gas-phase); however, model output was evaluated only for ~~five-six~~ hours through comparison to chamber measurements. In addition, we conducted a sensitivity analysis investigating a factor slowing down the heterogeneous chemistry and found that longer degradation time scales may occur, particularly in the aerosol phase ranging from 5 days (gas phase) to (7 days) (aerosol phase). ~~These-This~~ longer time scales is slightly larger are similar to

380 ~~than those that~~ of deposition (1-5 days) but ~~are is~~ slightly shorter than that of regional transport (10 days), suggesting that ~~both gas and aerosol some fraction of aerosol-phase LEV phases can be deposited locally but some fractions~~ may be transported regionally. However, these time scales remain to be evaluated using more extensive measurements from chambers and fire plumes. Additional sensitivity analyses using larger initial aerosol LEV concentrations in chamber simulations may result in longer degradation time scales of LEV aerosol concentration. Ultimately, implementation of the 0-D model development of this study into CTMs will help to clarify the regional transport and deposition of both LEV phases.

385 LEV degradation contributes to SOA formation that was quantified mainly through simulated SOA yields. Based on ~~56-h~~ degradation time scales, simulated SOA yields ranged from ~~5-4~~ to 32% and peaked in the first ~~1-12-2-34~~ minutes. Varying the heterogeneous chemistry rate by four orders of magnitude did not result in significantly different SOA yields (~~7-3214-33%~~), ~~but the decrease in the SOA yields was slower and extended to 4.5 days, consistent with the simulated degradation time scale of LEV in the same scenarios.~~ The total PM mass (determined as the ratio of total aerosol concentration to initial
390 LEV_A concentration) increased by ~~8-15%14%~~ in the first ~~7-minutes~~ six hours of all simulations and ~~continued to slowly increase to 18-29% at the end of the simulation period~~ remained essentially constant over time.

The addition of the multiphase LEV chemistry and the related G/P partitioning mechanism to the 0-D modelling framework has both direct and indirect effects on several gas-phase species. The average concentrations of OH, NO₃, O₃, HNO₃ and NO_z increased, while those of N₂O₅, NO_x and other VOC decreased. These changes are due to chemical reactions of the full
395 LEV chemistry which simultaneously consume and generate reactive species. Other species, included in the total VOC, are indirectly influenced by the LEV chemistry via competition for oxidants or via the oxidant concentration mediated by LEV chemistry. The effects of LEV chemistry on O₃ are complex: while it slows down its rate of formation by modulating NO_x and VOC concentrations, it increases the VOC/NO_x ratio, which in turn leads to higher O₃ (~~117-112~~ ppb) compared to the case without LEV chemistry (90 ppb).

400 LEV chemistry facilitates the conversion of NO_x to other reactive nitrogen forms (an increase of NO_z versus time at an average NO_z enhancement by 5 ppb). The effects of LEV chemistry on NO_z occur directly through LEVP5, a nitrated organic degradation product, and indirectly via generation of HNO₃ or consumption of N₂O₅, NO and NO₃ in chemical reactions. LEV chemistry drives changes in major air pollutants making it unwise to ignore it in future assessments of fire effects on tropospheric O₃, nitrogen ~~eyele-cycling~~ (via NO_z) and carbon ~~eyele-cycling~~ (via VOC and aerosol-phase
405 degradation products).

Future work should expand model development to include the degradation of the two LEV isomers (mannosan and galactosan) and to implement the full mechanism of anhydrosugar degradation into 3-D CTMs. The atmospheric implications of anhydrosugar degradation (i.e., SOA formation) and their tracing potential could then be evaluated more completely.

410

Author contribution. L. G. Suciu developed the LEVCHEM_v1 model, ran CMAQ simulations to provide initial conditions for LEVCHEM_v1 simulations, ran simulations, gathered data from chamber experiments, analysed simulations results,

evaluated model predictions, performed model sensitivity analysis, and wrote the manuscript. R. J. Griffin provided guidance for model development, evaluation, and sensitivity analysis, and critically reviewed the manuscript. C. A. Masiello provided
415 critical review of the manuscript.

Competing interests. The authors declare that they have no conflict of interest.

Code and data availability. The model version that was used in this study (*BOXMOXv1.7*) to develop *LEVCHEM_v1* is
420 available at the following website: <https://boxmodeling.meteo.physik.uni-muenchen.de/> under the Christoph Knote (LMU Munich, Germany) / Jérôme Barré (ECMWF, UK) licence. The exact version of the *BOXMOXv1.7* model that was updated (*LEVCHEM_v1*) as well as the input data and scripts used to run numerical chamber simulations of which results are presented in this paper are archived on Zenodo (<https://zenodo.org/record/3885786><https://zenodo.org/record/4215973>).

425 *Acknowledgements.* The authors wish to thank the BOXMOX developer, C. Knote, for the preliminary discussions regarding the development of a multiphase chemical mechanism. We are also grateful to Q. Z. Rasool and D. S. Cohan for sharing the data inputs needed for CMAQ simulations. Thanks to D. S. Cohan for useful discussions about model development and simulations. We thank the Department of Earth, Environmental and Planetary Sciences, Rice University, for providing the computational resources needed for the project and for IT support. We greatly appreciate the helpful comments and
430 suggestions from Andrew May and an anonymous reviewer of this manuscript.

References

- Alvarado, M. J., Wang, C. and Prinn, R. G.: Formation of ozone and growth of aerosols in young smoke plumes from biomass burning: 2. Three-dimensional Eulerian studies, *J. Geophys. Res.-Atmos.*, 114, D9, <https://doi.org/10.1029/2008JD011186>, 2009.
- Alvarado M. J., Lonsdale, C. R., Yokelson, R. J., Akagi, S., Coe, H., Craven, J. S., Fischer, E.V., McMeeking, G. R., Seinfeld, J. H., Soni, T., Taylor, J. W., Weise, D. R., and Wold, C.E.: Investigating the links between ozone and organic aerosol chemistry in a biomass burning plume from a prescribed fire in California chaparral, *Atmos. Chem. Phys.*, 15, 6667–6688, <https://doi.org/10.5194/acp-15-6667-2015>, 2015.
- 435 Arangio, A. M., Slade, J. H., Berkemeier, T., Pöschl, U., Knopf, D. A., and Shiraiwa, M.: Multiphase chemical kinetics of oh-OH radical uptake by molecular organic markers of biomass burning aerosols: humidity and temperature dependence, surface reaction, and bulk diffusion, *J. Phys. Chem., A* 119, 4533–4544, <https://doi.org/10.1021/jp510489z>, 2015.
- Atkinson, R., and Carter, W. P. L.: Kinetics and mechanisms of the gas-phase reactions of ozone with organic compounds under atmospheric conditions, *Chem. Rev.*, 84, 5, 437-470, <https://doi.org/10.1021/cr00063a002>, 1984.
- Bai, J., Sun, X., Zhang, C., Xu, Y., and Qi, C.: The OH-initiated atmospheric reaction mechanism and kinetics for

- levoglucosan emitted in biomass burning, *Chemosphere*, 93, 2004–2010, <https://doi.org/10.1016/j.chemosphere.2013.07.021>, 2013.
- Emmons, L. K., Walters, S., Hess, P. G., Lamarque, J.-F., Pfister, G. G., Fillmore, D., Granier, C., Guenther, A., Kinnison, D., Laepple, T., Orlando, J., Tie, X., Tyndall, G., Wiedinmyer, C., Baughcum, S. L., ~~and~~ Kloster, S.: Description and evaluation of the Model for Ozone and Related chemical Tracers, version 4 (MOZART-4), *Geosci. Model. Dev.*, 3, 43–67, <https://doi.org/10.5194/gmd-3-43-2010>, 2010.
- Fuchs, N. A. and Sutugin, A. G.: Highly dispersed aerosols, in *Topics in Current Aerosol Research. International Reviews in Aerosol Physics and Chemistry*, <https://doi.org/10.1016/B978-0-08-016674-2.50006-6>, 1971.
- 440 Gambaro, A., Zangrando, R., Gabrielli, P., Barbante, C., ~~and~~ Cescon, P.: Direct determination of levoglucosan at the picogram per milliliter level in antarctic ice by high-performance liquid chromatography/electrospray ionization triple quadrupole mass spectrometry, *Anal. Chem.*, 80, 1649–1655, <https://doi.org/10.1021/ac701655x>, 2008.
- Gensch, I., Sang-Arlt, X. F., Laumer, W., Chan, C. Y., Engling, G., Rudolph, J., ~~and~~ Kiendler-Scharr, A.: Using $\delta^{13}\text{C}$ of levoglucosan as a chemical clock, *Environ. Sci. Technol.*, 52, 11094–11101, <https://doi.org/10.1021/acs.est.8b03054>, 2018.
- 445 Gross, S., Ianonne, R., Xiao, S., ~~and~~ Bertram, A. K.: Reactive uptake studies of NO_3 and N_2O_5 on alkenoic acid, alkanolate, and polyalcohol substrates to probe nighttime aerosol chemistry, *Phys. Chem. Chem. Phys.*, 11, 7792–7803, <https://doi.org/10.1039/B904741G>, 2009.
- Hennigan, C.J., Sullivan, A. P., Collett, J. L., ~~and~~ Robinson, A. L.: Levoglucosan stability in biomass burning particles exposed to hydroxyl radicals, *Geophys. Res. Lett.*, 37, <https://doi.org/10.1029/2010GL043088>, 2010.
- Herron-Thorpe, F. L., Mount, G. H., Emmons, L. K., Lamb, B. K., Jaffe, D. A., Wigder, N. L., Chung, S. H., Zhang, R., Woelfle, M. D., ~~and~~ Vaughan, J. K.: Air quality simulations of wildfires in the Pacific Northwest evaluated with surface and satellite observations during the summers of 2007 and 2008, *Atmos. Chem. Phys.*, 14, 12533–12551, <https://doi.org/10.5194/acp-14-12533-2014>, 2014.
- Hoffmann, D., Tilgner, A., Iinuma, Y., ~~and~~ Herrmann, H.: Atmospheric stability of levoglucosan: a detailed laboratory and modeling study, *Environ. Sci. Technol.*, 44, 694–699, <https://doi.org/10.1021/es902476f>, 2010.
- 450 In, H.-J., Byun, D. W., Park, R. J., Moon, N.-K., Kim, S., ~~and~~ Zhong, S.: Impact of transboundary transport of carbonaceous aerosols on the regional air quality in the United States: A case study of the South American wildland fire of May 1998, *J. Geophys. Res.*, 112, <https://doi.org/10.1029/2006JD007544>, 2007.
- Jenkin, M.E., Saunders, S.M. and Pilling, M.J.: The tropospheric degradation of volatile organic compounds: a protocol for mechanism development, *Atmos. Environ.*, 31, 81–104, [https://doi.org/10.1016/S1352-2310\(96\)00105-7](https://doi.org/10.1016/S1352-2310(96)00105-7), 1997.
- Kawamura, K., Izawa, Y., Mochida, M., ~~and~~ Shiraiwa, T.: Ice core records of biomass burning tracers (levoglucosan and dehydroabietic, vanillic and p-hydroxybenzoic acids) and total organic carbon for past 300 years in the Kamchatka Peninsula, Northeast Asia, *Geochim. Cosmochim. Acta.*, 99, 317–329, <https://doi.org/10.1016/j.gca.2012.08.006>, 2012.
- 455 Kehrwald, N., Zangrando, R., Gabrielli, P., Jaffrezo, J.-L., Boutron, C., Barbante, C., ~~and~~ Gambaro, A.: Levoglucosan as a specific marker of fire events in Greenland snow, *Tellus B*, 64, <https://doi.org/10.3402/tellusb.v64i0.18196>, 2012.

- Kessler, S. H., Smith, J. D., Che, D. L., Worsnop, D. R., Wilson, K. R., and Kroll, J. H.: Chemical sinks of organic aerosol: kinetics and products of the heterogeneous oxidation of erythritol and levoglucosan, *Environ. Sci. Technol.*, 44, 7005–7010, <https://doi.org/10.1021/es101465m>, 2010.
- Knopf, D. A., Forrester, S. M., and Slade, J. H.: Heterogeneous oxidation kinetics of organic biomass burning aerosol surrogates by O₃, NO₂, N₂O₅, and NO₃, *Phys. Chem. Chem. Phys.*, 13, 21050, <https://doi.org/10.1039/c1cp22478f>, 2011.
- Knote, C., Tuccella, P., Curci, G., Emmons, L., Orlando, J. J., Madronich, S., Baró, R., Jiménez-Guerrero, P., Luecken, D., Hogrefe, C., Forkel, R., Verhahn, J., Hirtl, M., Pérez, J. L., San José, R., Giordano, L., Brunner, D., Yahya, K., and Zhang, Y.: Influence of the choice of gas-phase mechanism on predictions of key gaseous pollutants during the AQMEII phase-2 intercomparison, *Atmos. Environ.*, 115, 553–568, <https://doi.org/10.1016/j.atmosenv.2014.11.066>, 2015.
- [Kulmala, M. and Wagner, P. E.: Mass accommodation and uptake coefficients - a quantitative comparison, *J. Aerosol Sci.*, 32, 7, 833–841, \[https://doi.org/10.1016/S0021-8502\\(00\\)00116-6\]\(https://doi.org/10.1016/S0021-8502\(00\)00116-6\), 2001.](#)
- 460 Lai, C., Liu, Y., Ma, J., Ma, Q., and He, H.: Degradation kinetics of levoglucosan initiated by hydroxyl radical under different environmental conditions, *Atmos. Environ.*, 91, 32–39, <https://doi.org/10.1016/j.atmosenv.2014.03.054>, 2014.
- [May, A. A., Saleh, R., Hennigan, C. J., Donahue, N. M. and Robinson, A. L.: Volatility of organic molecular markers used for source apportionment analysis: measurements and implications for atmospheric lifetime, *Environ. Sci. Technol.*, 46, 22, 12435–12444, <https://doi.org/10.1021/es302276t>, 2012.](#)
- 465 May, A. A., Levin, E. J. T., Hennigan, C. J., Riipinen, I., Lee, T., Collett, J. L., Jimenez, J. L., Kreidenweis, S. M., and Robinson, A. L.: Gas-particle partitioning of primary organic aerosol emissions: 3. Biomass burning, *J. Geophys. Res.-Atmos.*, 118, 11,327–11,338, <https://doi.org/10.1002/jgrd.50828>, 2013.
- [Pratap, V., Chen Y., Yao G. and Nakao S.: Temperature effects on multiphase reactions of organic molecular markers: A modeling study, *Atmos. Environ.*, 179, 40–48, <https://doi.org/10.1016/j.atmosenv.2018.02.009>, 2018.](#)
- 470 [Pratap, V., Bian, Q., Kiran, S. A., Hopke, P. K., Pierce, J. R. and Nakao, S.: Investigation of levoglucosan decay in wood smoke smog-chamber experiments: The importance of aerosol loading, temperature, and vapor wall losses in interpreting results, *Atmos. Environ.*, 199, 224–232, <https://doi.org/10.1016/j.atmosenv.2018.11.020>, 2019.](#)
- Pye, H. O. T. and Pouliot, G. A.: Modeling the role of alkanes, polycyclic aromatic hydrocarbons, and their oligomers in secondary organic aerosol formation, *Environ. Sci. Technol.*, 46, 11, 6041–6047, <https://doi.org/10.1021/es300409w>, 2012.
- 475 Rasool, Q. Z., Zhang, R., Lash, B., Cohan, D. S., Cooter, E. J., Bash, J. O., and Lamsal, L. N.: Enhanced representation of soil NO emissions in the Community Multiscale Air Quality (CMAQ) model version 5.0.2, *Geosci. Model. Dev.*, 9, 3177–3197, <https://doi.org/10.5194/gmd-9-3177-2016>, 2016.
- Sandu, A. and Sander, R.: Technical note: Simulating chemical systems in Fortran90 and Matlab with the Kinetic PreProcessor KPP-2.1, *Atmos. Chem. Phys.*, 6, 187–195, <https://doi.org/10.5194/acp-6-187-2006>, 2006.
- 480 Saunders, S. M, Jenkin, M. E., Derwent, R. G., and Pilling, M. J.: Protocol for the development of the Master Chemical Mechanism, MCM v3 (Part A): tropospheric degradation of non-aromatic volatile organic compounds, *Atmos. Chem. Phys.*, 3, 161–180, <https://doi.org/10.5194/acp-3-161-2003>, 2003.

Seinfeld, J. H. and Pandis, S. N.: Atmospheric chemistry and physics: from air pollution to climate change, John Wiley & Sons, Inc, Hoboken, NJ, 2006.

485 Simon, H. and Bhawe, V. P.: Simulating the Degree of Oxidation in Atmospheric Organic Particles. *Environ. Sci. Technol.*, 46, 1, 331-339. <https://doi.org/10.1021/es202361w>, 2012.

Slade, J. H. and Knopf, D. A.: Multiphase OH oxidation kinetics of organic aerosol: The role of particle phase state and relative humidity, *Geophys. Res. Lett.*, 41, 5297–5306, <https://doi.org/10.1002/2014GL060582>, 2014.

490 Stefenelli, G., Jiang, J., Bertrand, A., Bruns, E. A., Pieber, S. M., Baltensperger, U., Marchand, N., Aksoyoglu, S., Prévôt, A. S. H., Slowik, J. G., and El Haddad, I.: Secondary organic aerosol formation from smoldering and flaming combustion of biomass: a box model parametrization based on volatility basis set, *Atmos. Chem. Phys.*, 19, 11461–11484, <https://doi.org/10.5194/acp-19-11461-2019>, 2019.

Suciu, L. G., Masiello, C. A. and Griffin, R. J.: Anhydrosugars as tracers in the Earth system, *Biogeochemistry*, 146, 3, 209-256, <https://link.springer.com/article/10.1007/s10533-019-00622-0>, 2019.

495 Sullivan, A. P., May, A. A., Lee, T., McMeeking, G. R., Kreidenweis, S. M., Akagi, S. K., Yokelson, R. J., Urbanski, S. P., and Collett Jr., J. L.: Airborne characterization of smoke marker ratios from prescribed burning, *Atmos. Chem. Phys.*, 14, 10535–10545, <https://doi.org/10.5194/acp-14-10535-2014>, 2014.

You, C., and Xu, C.: Review of levoglucosan in glacier snow and ice studies: Recent progress and future perspectives, *Sci. Total Environ.*, 616-617, 1533–1539, <https://doi.org/10.1016/j.scitotenv.2017.10.160>, 2018.

500 **Table 1 Homogeneous gas-phase mechanism**

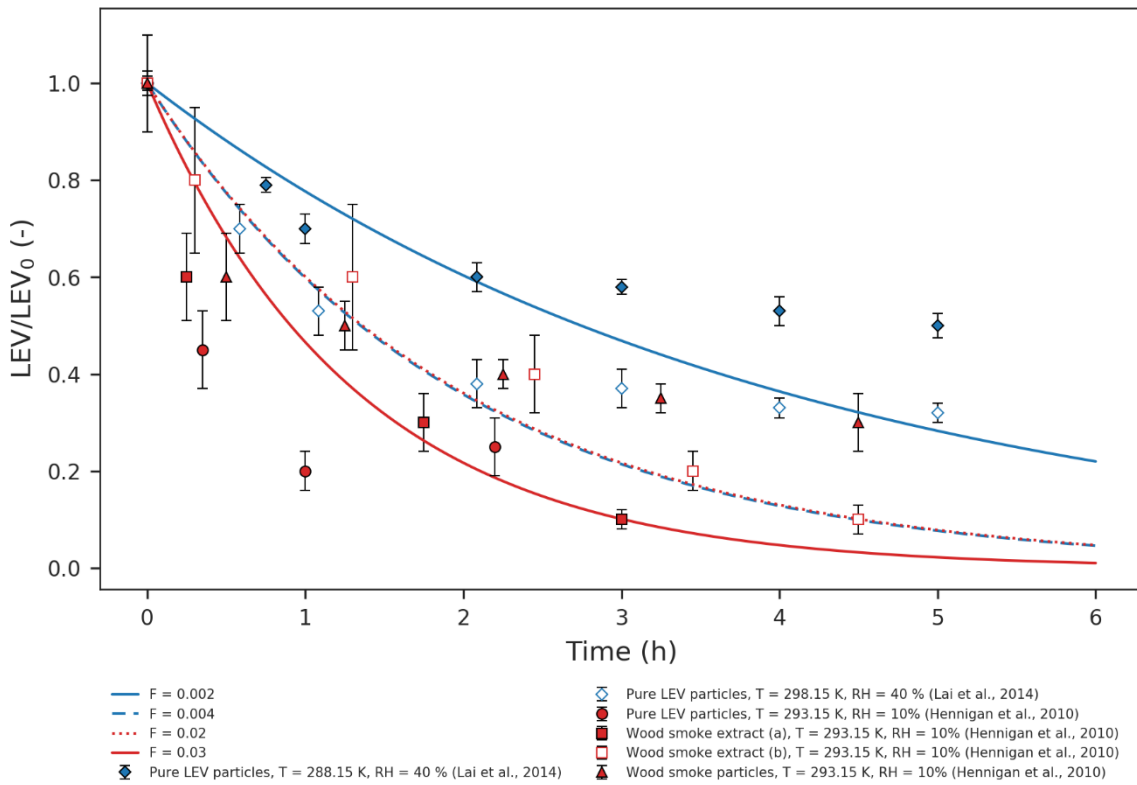
Chemical reaction	Reference	Reaction rate coefficient [cm ³ molec ⁻¹ s ⁻¹]	Reference
1. LEV_G + OH {+ O ₂ } → LEVRO2_G + H ₂ O	Bai et al. (2013); Jenkin et al. (1997)	2.21 x 10 ⁻¹²	Bai et al. (2013)
2. LEVRO2_G + NO → LEVRO_G + NO ₂	Saunders et al. (2003)	2.54 x 10 ⁻¹² exp (360/T)	Saunders et al. (2003)
3. LEVRO_G + O ₂ → LEVP1_G + HO ₂	Saunders et al. (2003)	1.00 x 10 ⁻¹⁴	Seinfeld and Pandis (2006)
4. LEVRO2_G + H ₂ O → LEVP2_G + OH + H ₂ O	Jenkin et al. (1997); Bai et al. (2013)	1.00 x 10 ⁻¹⁷	Jenkin et al. (1997)
5. LEVP2_G + LEV → LEVP3_G	Bai et al. (2013)	3.10 x 10 ⁻¹⁰ exp (155/T)	Calculated in this study
6. LEVRO2_G + M → LEVP4_G + HO ₂ + M	Bai et al. (2013)	5.76 x 10 ⁻¹² exp (71/T)	Calculated in this study
7. 2LEVRO2_G → 2LEVRO_G + O ₂	Saunders et al. (2003)	2.70 x 10 ⁻¹²	Jenkin et al. (1997)
8. LEVRO2_G + XO ₂ → LEVRO_G + ROR + O ₂	Saunders et al. (2003)	2.70 x 10 ⁻¹²	Jenkin et al. (1997)
9. LEVRO2_G + HO ₂ → LEVROOH_G + O ₂	Saunders et al. (2003)	2.91 x 10 ⁻¹³ exp (1300/T)	Saunders et al. (2003)
10. LEVROOH_G + OH → LEVRO2_G + H ₂ O	Emmons et al. (2010)	3.80 x 10 ⁻¹² exp (200/T)	Emmons et al. (2010)
11. LEV_G + NO ₃ {+ O ₂ } → LEVRO2_G + HNO ₃	Jenkin et al. (1997); Knopf et al. (2011)	5.80 x 10 ⁻¹⁶	CB05TUCL_EPA (R77)
12. LEV_G + O ₃ {+ O ₂ } → LEVRO2_G + O ₂ + OH	Jenkin et al. (1997); Atkinson and Carter (1984)	1.20 x 10 ⁻¹⁴ exp (2630/T)	CB05TUCL_EPA (R122)
13. LEV_G + N ₂ O ₅ → LEVP5_G + HNO ₃	Gross et al. (2009)	1.29 x 10 ⁻¹⁴	Calculated this study

{ } Species concentration not included in the reaction rate (i.e., reaction of LEV_G radical with O₂ is assumed to be instantaneous)

Table 2 Heterogeneous mechanism

Chemical reaction	Reference	Uptake coefficient ^a	Reference
1. LEV_A {+ OH} → LEVR_A + H ₂ O	Bai et al. (2013); Jenkin et al. (1997)	0.91	Kessler et al. (2010)
2. LEVR_A {+ O ₂ } → LEVRO2_A	Saunders et al. (2003)	0.41	Calculated this study
3. LEVRO2_A {+ NO} → LEVRO_A + NO ₂	Saunders et al. (2003)	0.36	Calculated this study
4. LEVRO_A {+O ₂ } → LEVP1_A + O ₂	Saunders et al. (2003)	0.41	Calculated this study
5. LEVRO2_A {+ H ₂ O} → LEVP2_A + OH + H ₂ O	Bai et al. (2013); Jenkin et al. (1997)	0.22	Calculated this study
6. LEVP2_A {+ LEV_G} → LEVP3_A	Bai et al. (2013)	0.92	Calculated this study
7. LEVRO2_A {+ LEVRO2_G} → LEVRO_A + LEVRO_G + O ₂	Saunders et al. (2003)	0.85	Calculated this study
8. LEVRO2_A {+ HO ₂ } → LEVROOH_A + O ₂	Saunders et al. (2003)	0.33	Calculated this study
9. LEVROOH_A {+ OH} → LEVRO2_A + H ₂ O	Emmons et al. (2010)	0.27	Calculated this study
10. LEV_A {+ OH} → LEVP6_A + LEVR1_A + H ₂ O	Kessler et al. (2010)	0.27	Calculated this study
11. LEVR1_A {+O ₂ } → LEVP7_A + HO ₂	Saunders et al. (2003)	0.41	Calculated this study
12. LEV_A {+ NO ₃ } → LEVR_A + HNO ₃	Jenkin et al. (1997); Knopf et al. (2011)	1.29	Knopf et al. (2011)
13. LEV_A {+ O ₃ } → LEVR_A + O ₂ + OH	Jenkin et al. (1997); Atkinson and Carter (1984)	0.013	Knopf et al. (2011)
14. LEV_A {+ N ₂ O ₅ } → LEVP5_A + HNO ₃	Gross et al. (2009)	0.027	Knopf et al. (2011)

^aThe uptake coefficient used in the calculation of the heterogeneous reaction rate coefficient (see eq. 5)



505

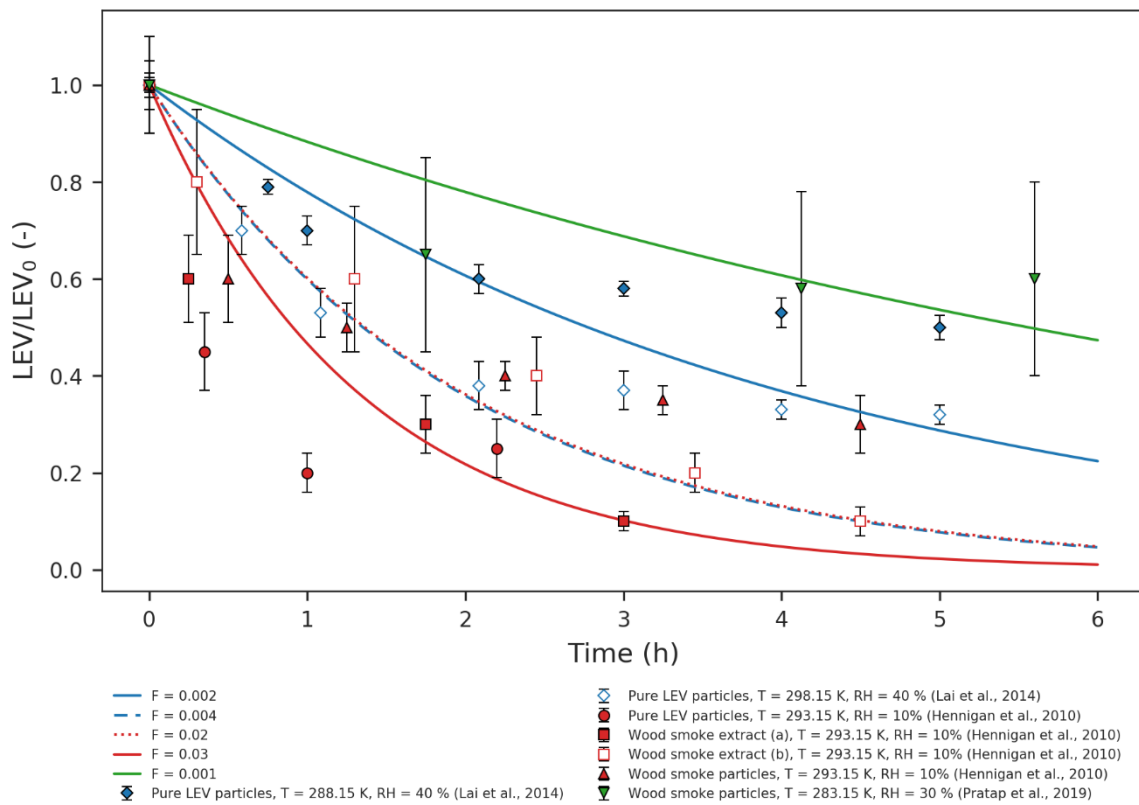
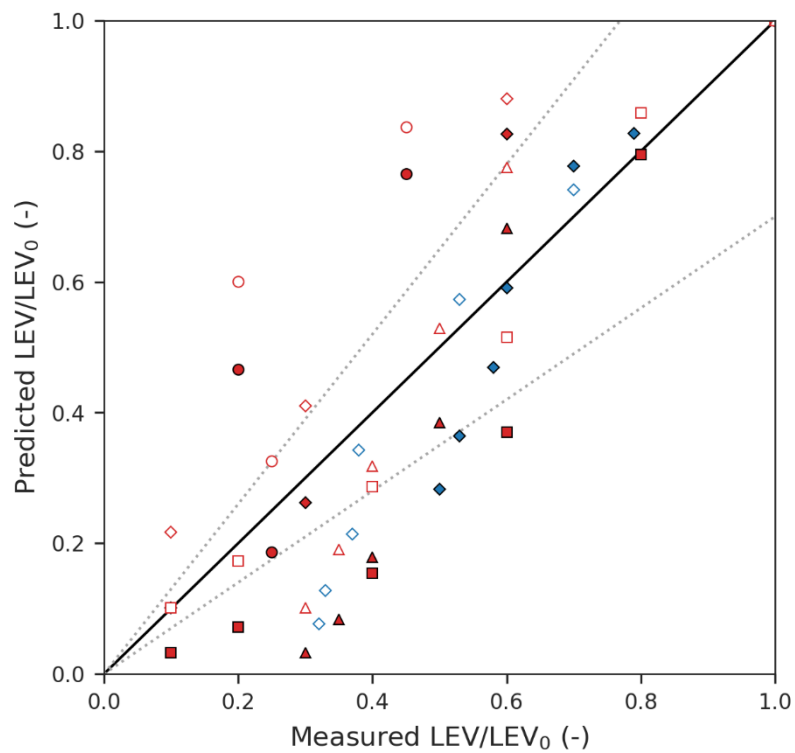


Figure 1 Simulated LEV degradation (lines) and measured LEV degradation (points); Color represents conditions from different chamber experiments taken from ~~two~~ three studies (red – Hennigan et al. (2010) ~~and~~, blue – Lai et al. (2014) ~~and~~ green – Pratap et al. (2019)) used in the simulations. LEV concentration is normalized by the initial concentration (LEV/LEV_0).



- ◆ Pure LEV particles, T = 288.15 K, RH = 40 % (Lai et al., 2014)
- ◇ Pure LEV particles, T = 298.15 K, RH = 40 % (Lai et al., 2014)
- Pure LEV particles, T = 293.15 K, RH = 10% (Hennigan et al., 2010)
- Pure LEV particles, T = 293.15 K, RH = 10% (Hennigan et al., 2010)
- ◆ Wood smoke extract (a), T = 293.15 K, RH = 10% (Hennigan et al., 2010)
- ◇ Wood smoke extract (a), T = 293.15 K, RH = 10% (Hennigan et al., 2010)
- Wood smoke extract (b), T = 293.15 K, RH = 10% (Hennigan et al., 2010)
- Wood smoke extract (b), T = 293.15 K, RH = 10% (Hennigan et al., 2010)
- ▲ Wood smoke particles, T = 293.15 K, RH = 10% (Hennigan et al., 2010)
- △ Wood smoke particles, T = 293.15 K, RH = 10% (Hennigan et al., 2010)

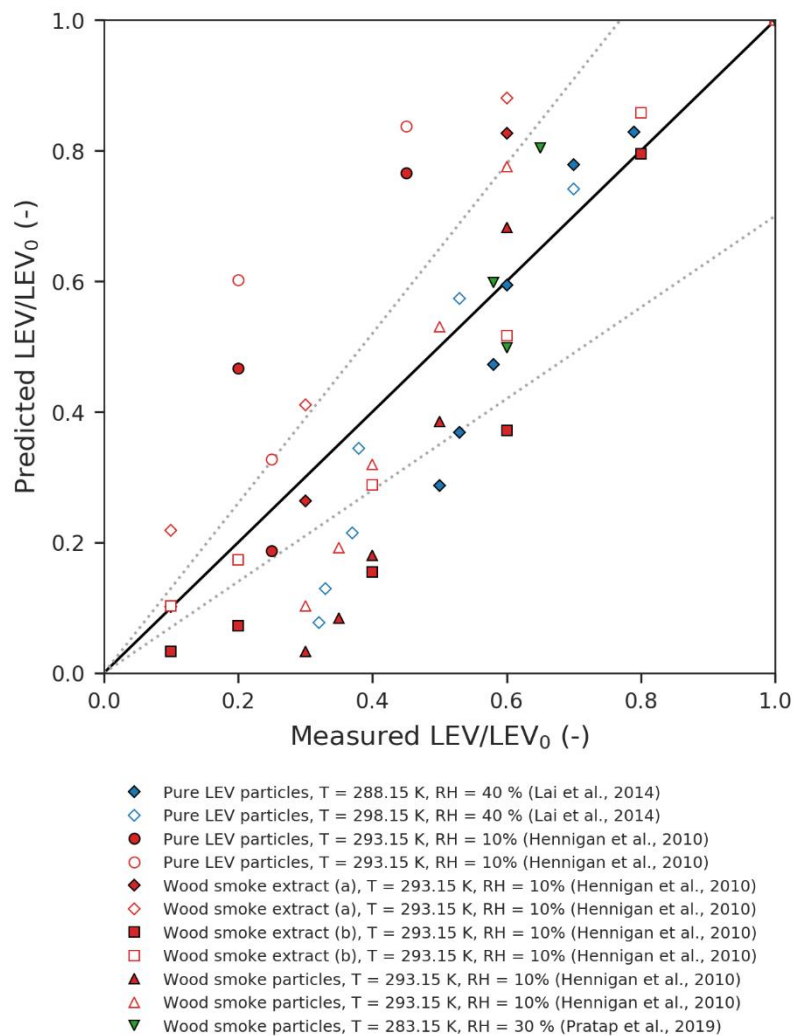


Figure 2 Parity plot of predicted versus measured LEV concentration (normalized by the initial concentration). The dotted lines represent the $\pm 30\%$ error margins.

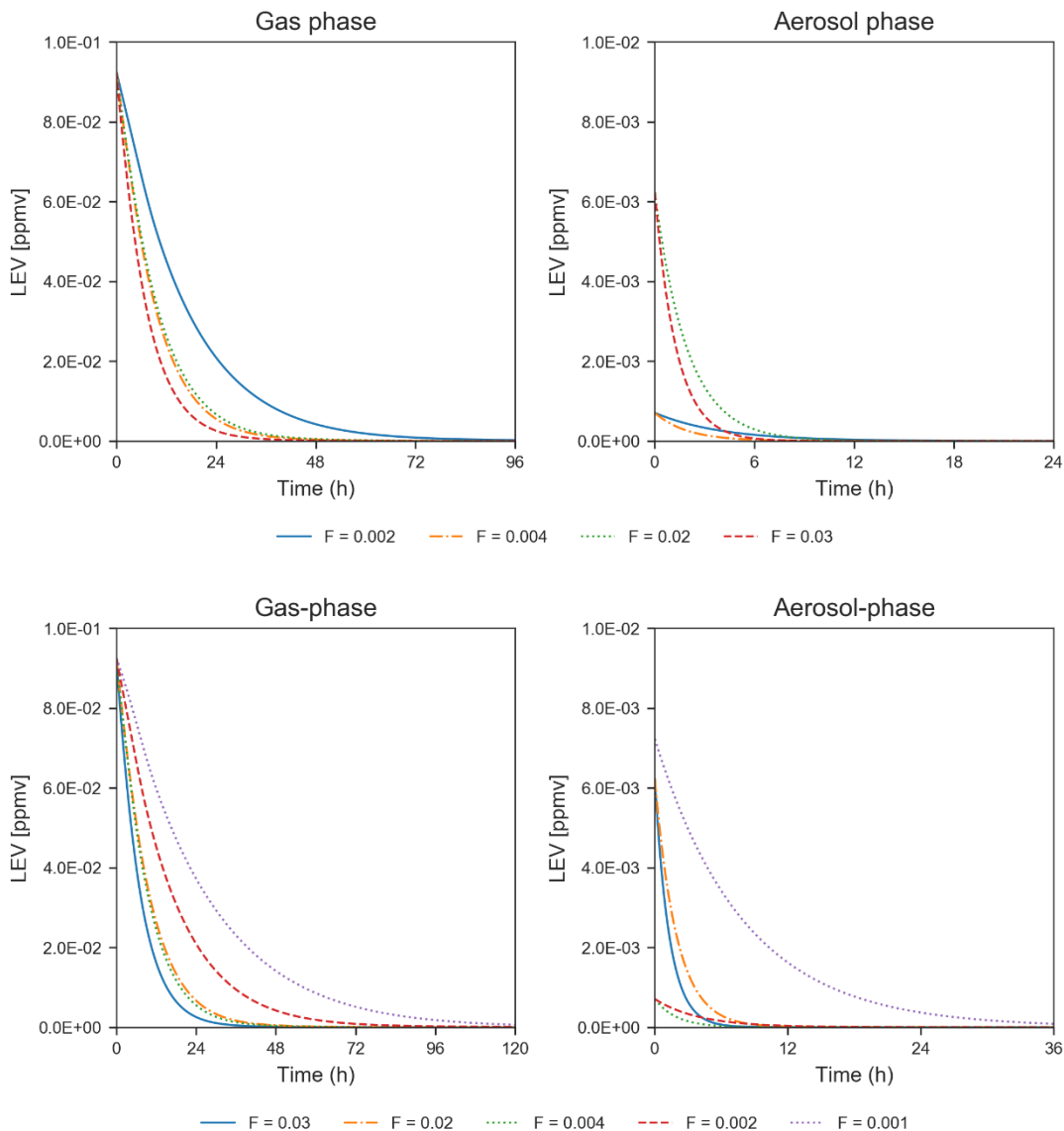
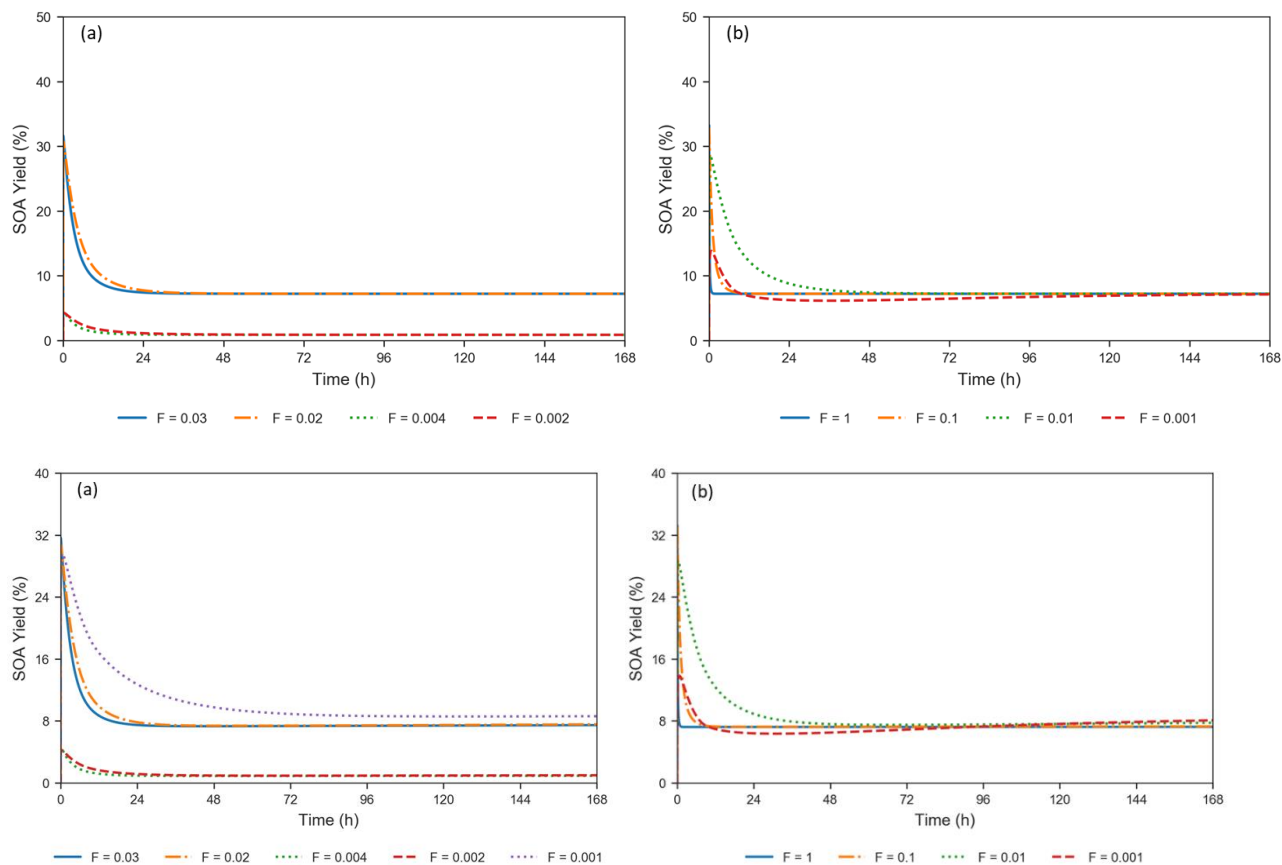


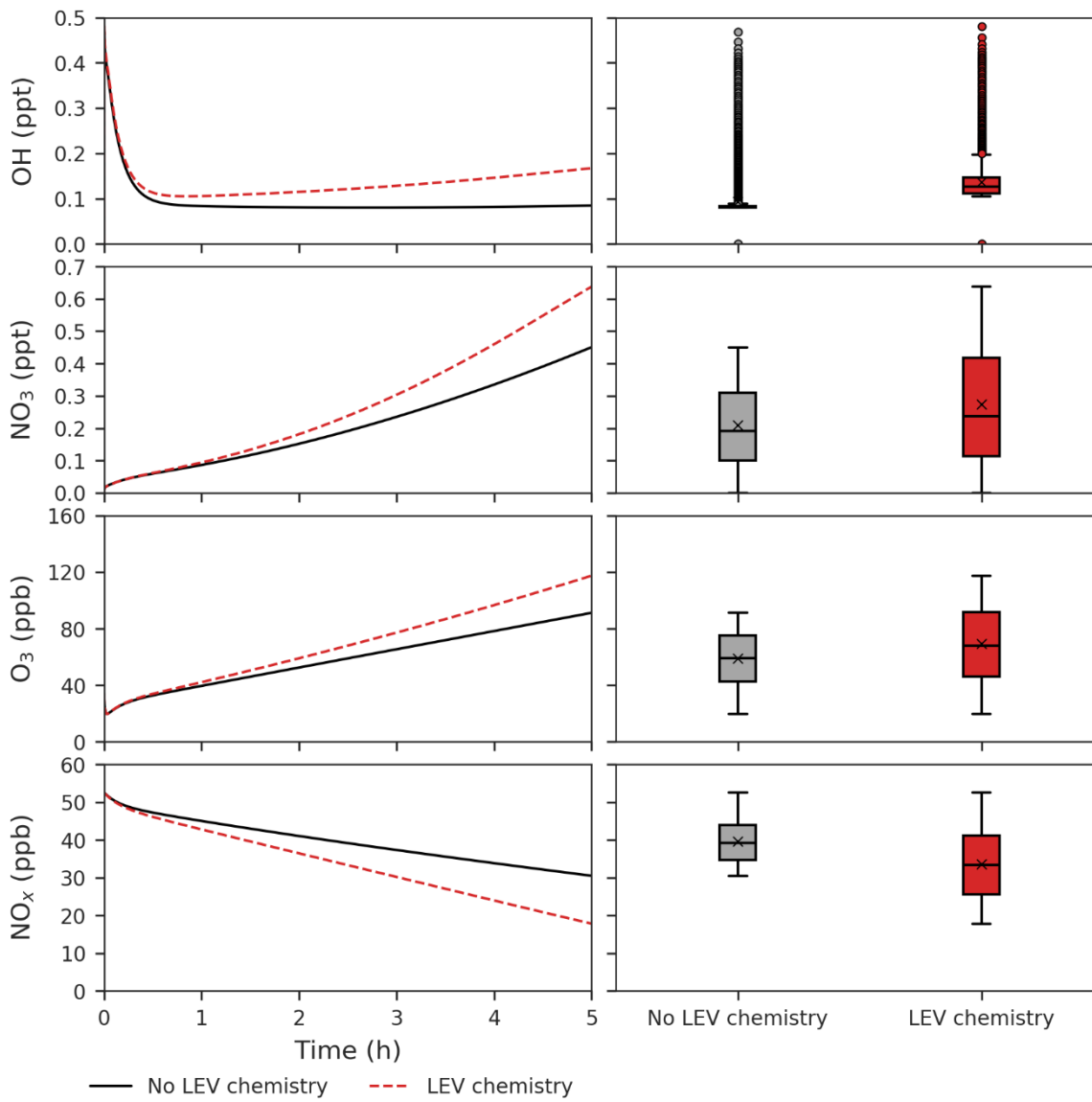
Figure 3 Degradation of LEV ~~in simulations at constant mass accommodation coefficient ($\alpha = 0.001$)~~ (conditions from Hennigan et al. (2010) when ~~F=0.02 and 0.03~~ and $\alpha = 0.1$, and from Lai et al. (2014) when ~~F=0.002 and 0.004~~ and $\alpha = 0.01$, and from Pratap et al. (2019) when ~~F = 0.003~~ and $\alpha = 0.01$). Note the change in the scale of the axes between the two panels.

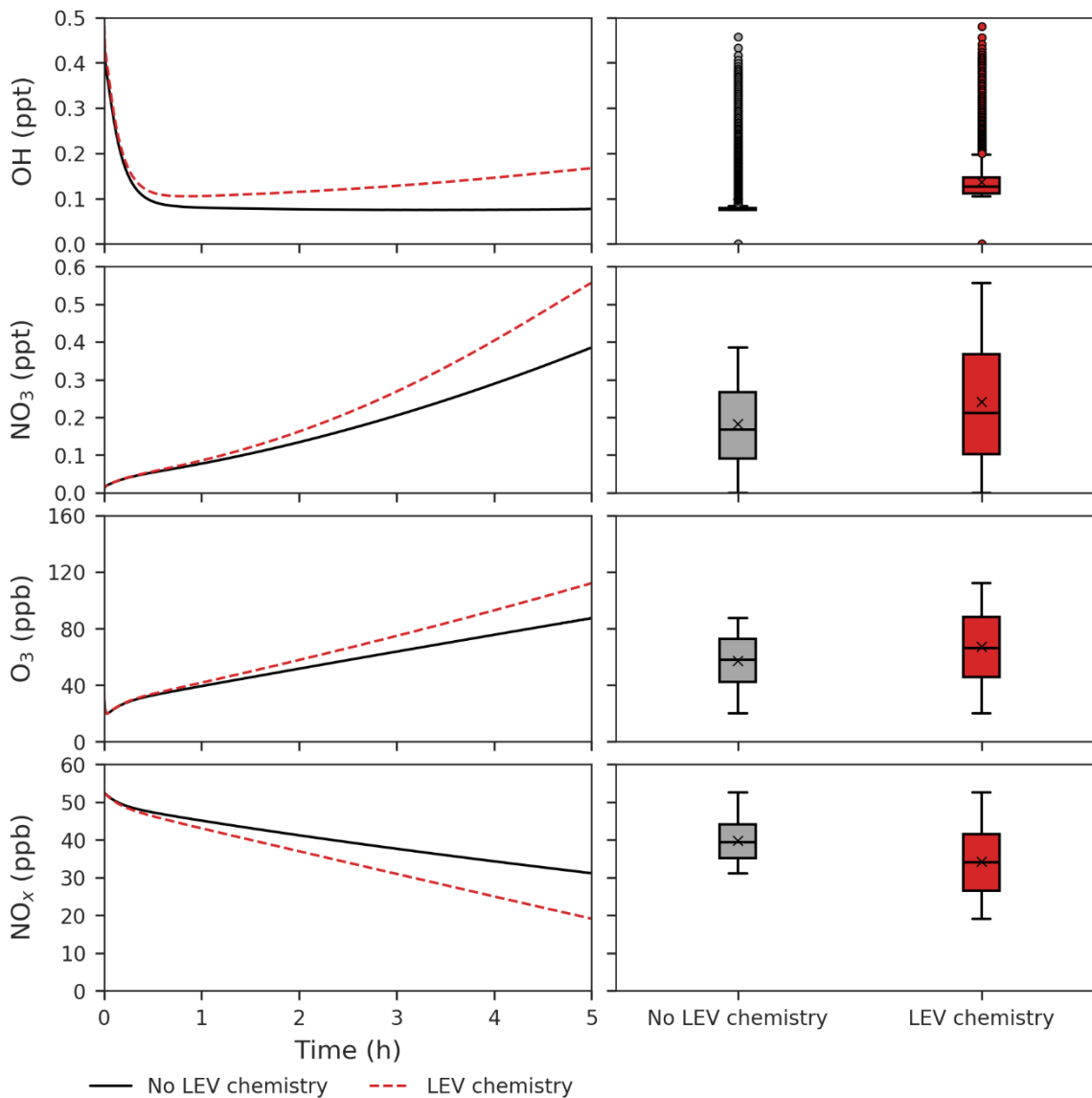
520



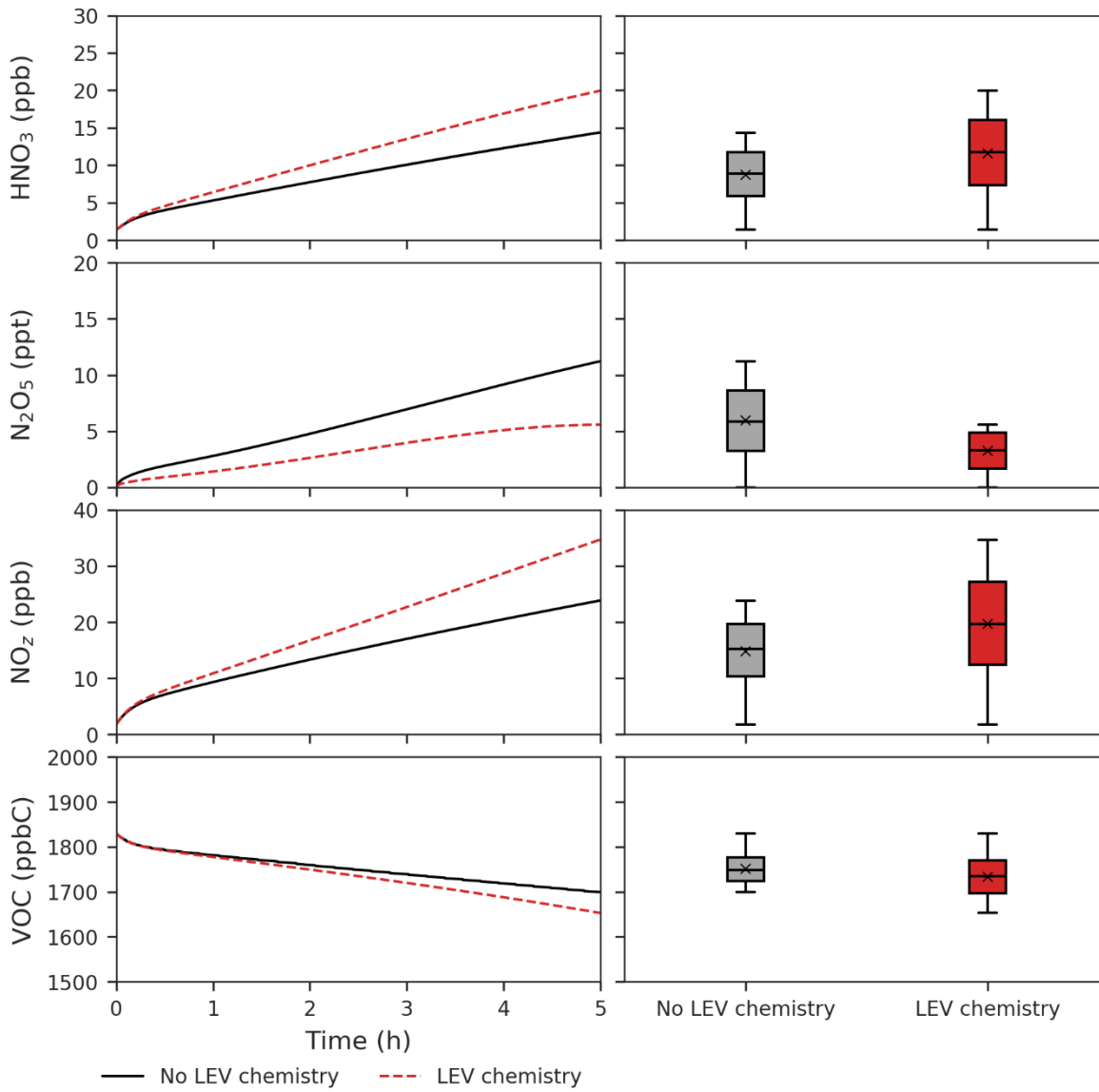
525 **Figure 4 (a) Evolution of SOA yields from LEV degradation using valid simulations at constant mass accommodation coefficient ($\alpha = 0.001$) (conditions from Hennigan et al. (2010) when $F=0.02$ and 0.03 and $\alpha = 0.1$, and from Lai et al. (2014) when $F=0.002$ and 0.004 and $\alpha = 0.01$), and from Pratap et al. (2019) when $F = 0.001$ and $\alpha = 0.01$). (b) Effect of varying the heterogeneous reaction rate coefficient by 4 orders of magnitude, at constant mass accommodation coefficient ($\alpha = 0.001$) (conditions from Hennigan et al. (2010)).**

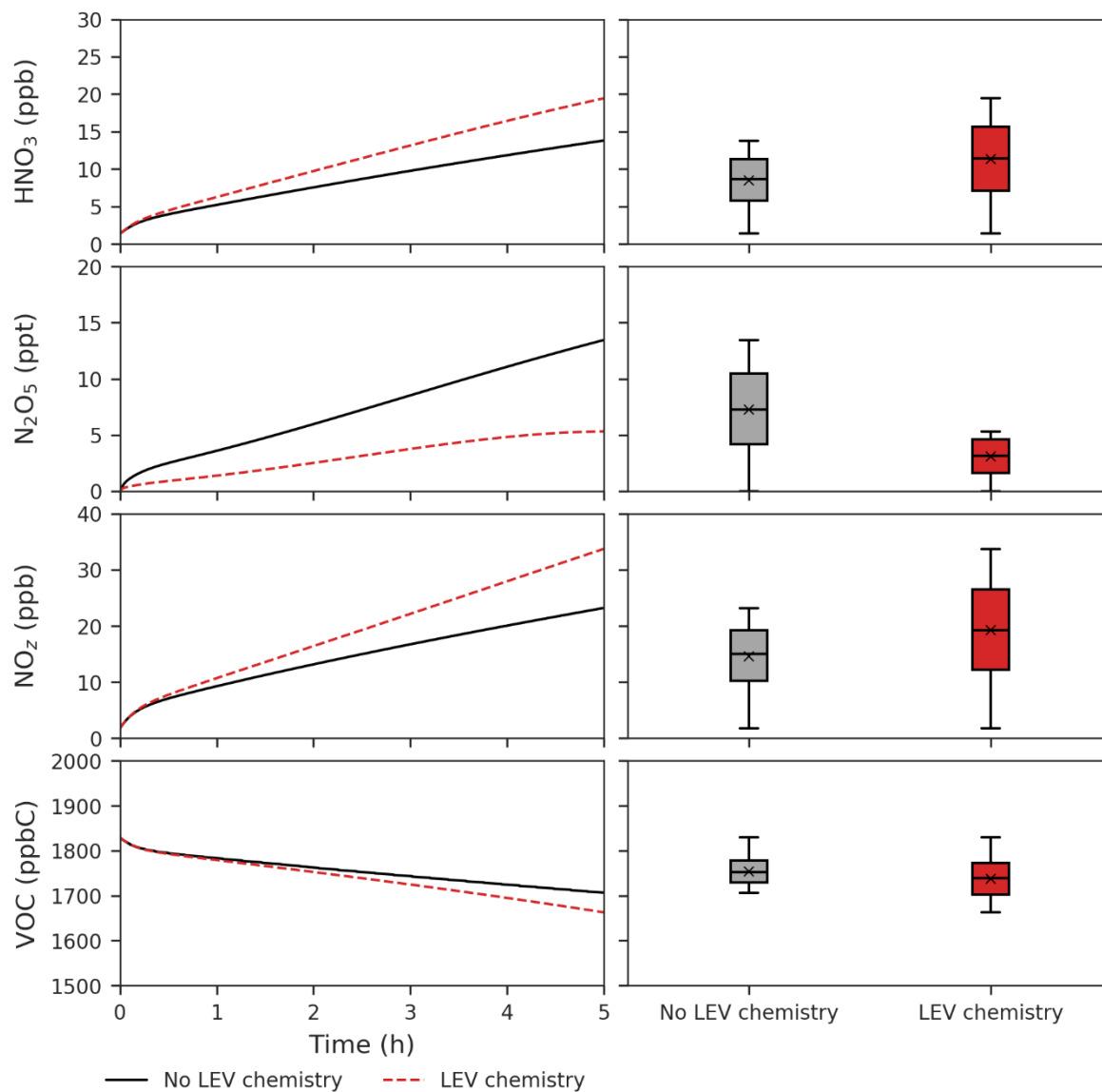
530





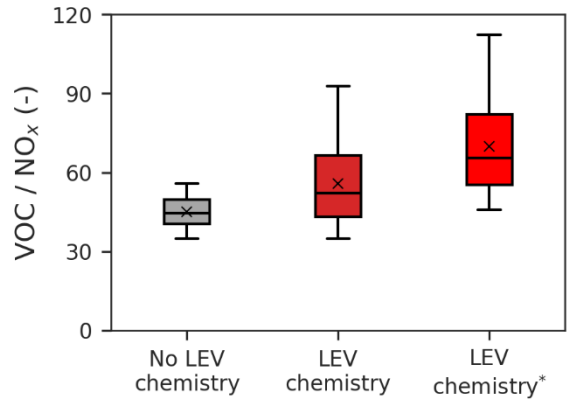
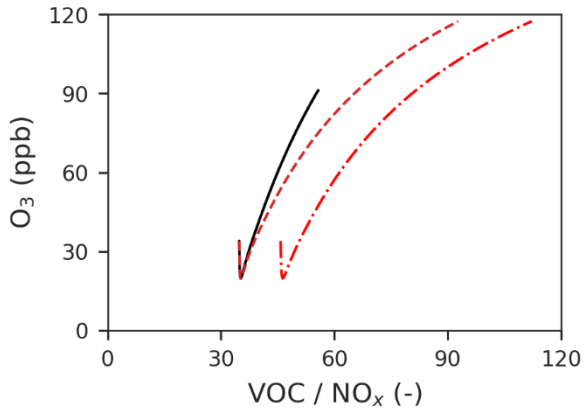
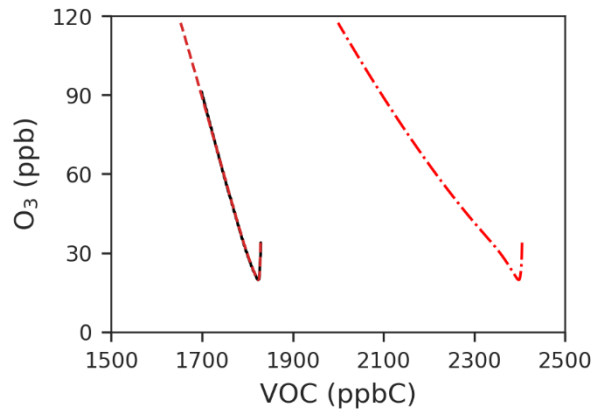
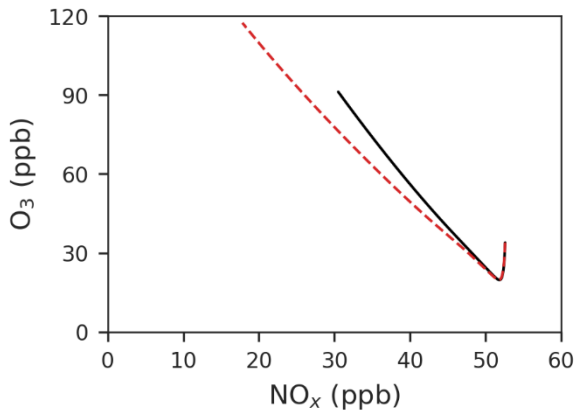
535 **Figure 5** Effects of LEV chemistry on OH, NO₃, O₃ and NO_x (in red, relative to the case without LEV chemistry shown in black or grey). The time series represent averages of simulations performed with LEV chemistry (dashed red line) and without LEV chemistry (black line) over the 5-h time scale. The box plots show the distributions of the species concentration for the entire 5 hours. Note that findings shown here are determined over a range of F values depending on experimental conditions.



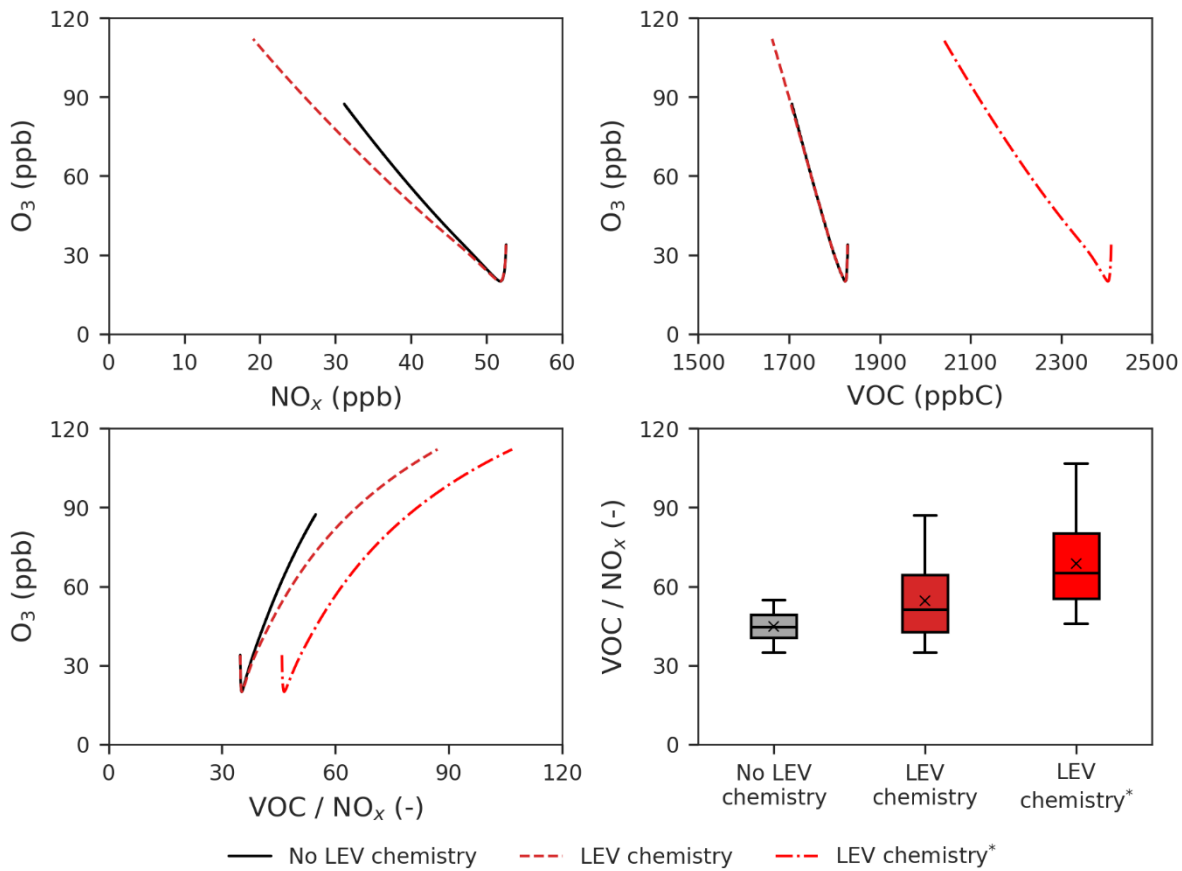


540 **Figure 6** Effects of LEV chemistry on HNO₃, N₂O₅, NO_z and VOC (in red, relative to the case without LEV chemistry shown in black or grey). The time series represent averages of simulations performed with LEV chemistry (dashed red line) and without LEV chemistry (black line) over the 5-h time scale. The box plots show the distributions of the species concentration for the entire 5 hours. Note that findings shown here are determined over a range of F values depending on experimental conditions.

545

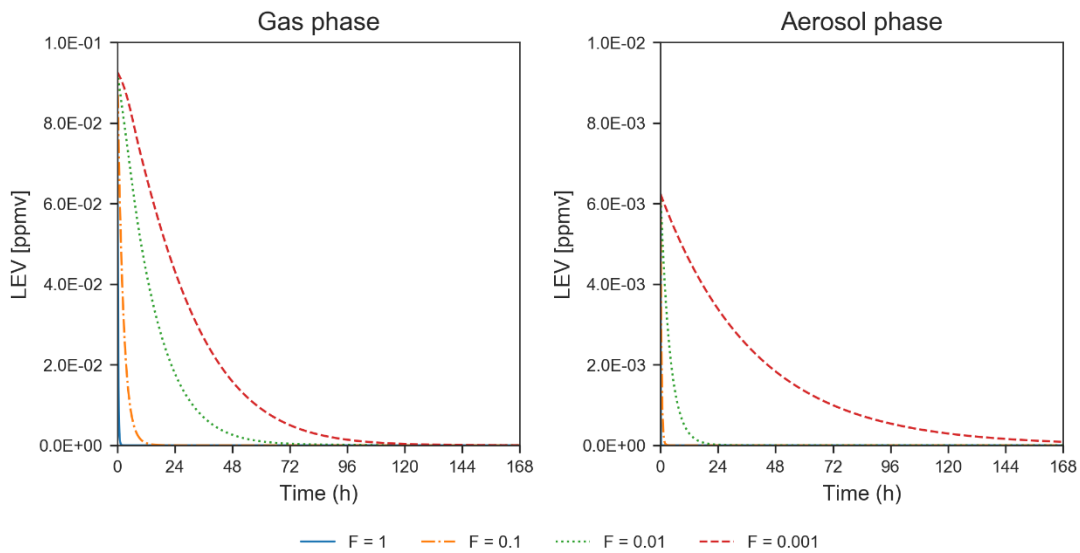


— No LEV chemistry - - - LEV chemistry - · - LEV chemistry*



550 **Figure 7 Effects of LEV chemistry on the O_3 versus NO_x , O_3 versus VOC and O_3 versus VOC/ NO_x ratio relationships and on the VOC/ NO_x ratio. The two cases in red (with LEV chemistry) refer to the two ways in which VOC was determined (with/without LEV_G and LEV_A). The asterisk refers to the inclusion of LEV_G and LEV_A in the total VOC. All the plots show simulation results at the 5-h time scale. Note that findings shown here are determined over a range of F values depending on experimental conditions.**

555



560

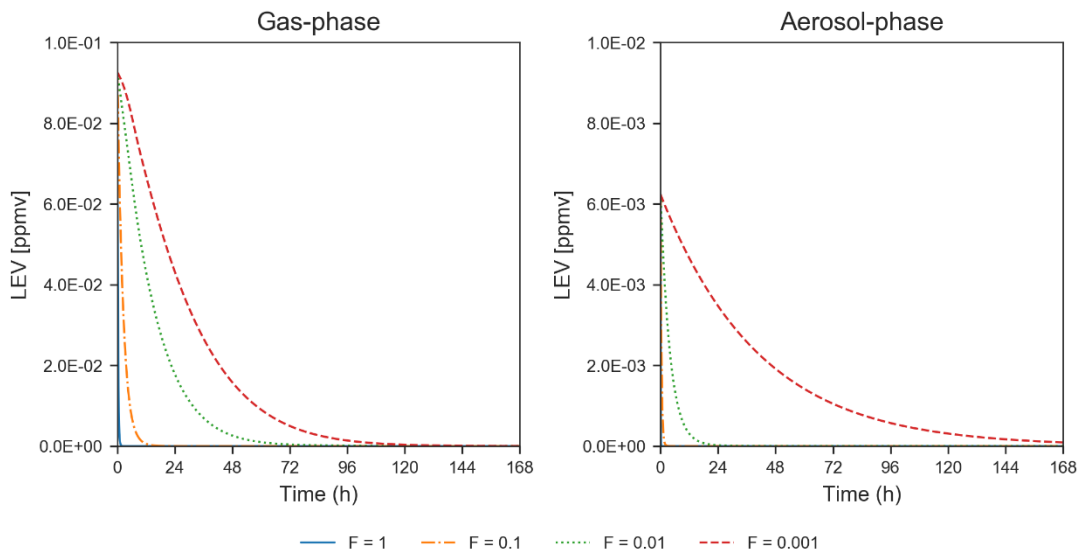


Figure 8 Degradation of LEV by varying the heterogeneous reaction rate coefficient by 4 orders of magnitude, at constant mass accommodation coefficient ($\alpha = 0.001$) and $C_i^* = 13 \mu\text{g m}^{-3}$ (conditions from Hennigan et al. (2010)). Note that the y-axis scale changes between the concentrations presented for the two phases.

565